JOURNAL OF THE AERONAUTICAL SCIENCES

VOLUME 10 APRIL, 1943 NUMBER 4

General Instability of Monocoque Cylinders

N. J. Hoff*

Polytechnic Institute of Brooklyn

SUMMARY

The different types of general instability already discussed in literature are critically reviewed. The writer's earlier theoretic calculations of the critical load of the inward bulge type of general instability are revised in the light of the experimental data of the GALCIT investigation. A new simple formula is derived which is in reasonable agreement with experiment.

TYPES OF GENERAL INSTABILITY

GENERAL INSTABILITY is defined as the simultaneous buckling of the longitudinal and the transverse reinforcing elements of a monocoque structure. The definition is meaningless unless the monocoque has both longitudinal and transverse reinforcements, and only such monocoques are considered in the present paper. For this reason the word "monocoque" can be used in place of the more cumbersome "semimonocoque" or "reinforced monocoque" without incurring any danger of misunderstanding.

There are several known types of instability which conform with the above definition, and undoubtedly additional ones will be described in the future. They vary considerably in the value of the critical loads and in the pattern of the distortions. To facilitate an understanding of the problems involved it appears advantageous to adopt a different name for each of the various types of general instability. Such names are suggested below for the types already described in literature, and their characteristic features are briefly discussed.

Flattening in Compression

Wang[13] showed that a monocoque cylinder loaded with uniformly distributed compressive forces may fail by flattening. "Flattening" means that the originally circular rings (transverse reinforcing elements) distort to ellipses and the originally straight stringers (longitudinal reinforcing elements) to sine curves of one or more half-wave lengths (see Fig. 1). The critical load

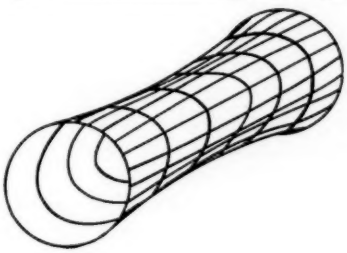

FIG. 1. Flattening type of general instability.

was calculated by the Rayleigh-Ritz-Timoshenko method. The distortions of the rings and stringers were assumed to be inextensional and were represented by trigonometric series. The sheet-metal covering was assumed to be infinitely thin and the strain energy stored in it was neglected.

Experimental evidence of this type of general instability is not available. It might be obtained with monocoques that are so proportioned that the buckling stress of their panels of sheet is much smaller than the buckling stress corresponding to general instability, provided that the reduction in the resistance to shear does not result in some form of torsional instability. If, however, the panels of sheet are still in the unbuckled state when general instability should occur according to Wang's calculations, the strain energy due to shear in the sheet covering is not negligibly small, and it is likely to influence greatly both the critical load and the distortion pattern.

Diamond Pattern in Compression

The deflections are sinusoidal in both the longitudinal and circumferential directions and usually consist of several half-waves in either direction (see Fig. 2). The pattern is much the same as the one well known from the buckling of thin-walled nonreinforced circular cylinders. By definition the half-wave length in the longitudinal direction must be greater than the spacing of the rings if the buckling is to be classified as general

Presented at the Structures Session, Eleventh Annual Meeting, I.Ae.S., New York, January 25–29, 1943.

* Assistant Professor of Aeronautical Engineering.

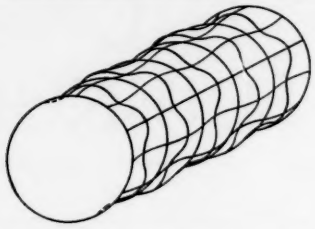

FIG. 2. Diamond pattern type of general instability.

instability. The flattening discussed previously is just that special case of the diamond pattern when the number of half-waves is four in the circumferential direction.

The buckling load of the diamond pattern type of general instability was calculated by Flügge,[3] Dschou,[2] Taylor,[11] and Ryder.[9] The problem is also discussed by Timoshenko.[12] In all these calculations the actual monocoque is replaced by an equivalent orthotropic shell—that is, by one that has different but uniformly distributed bending rigidities in the longitudinal and circumferential directions. The shearing stresses in the sheet covering are not disregarded.

Experiments carried out by Nissen[8] with monocoque cylinders covered with corrugated sheet showed good agreement with Dschou's theoretic formulas if experimentally determined values were used for the stiffness.

Many attempts were made to use the theoretic formulas derived for the diamond-type buckling in compression for the calculation of the critical stresses of monocoque cylinders tested in bending. The basis for such a procedure is the argument that the critical stress in bending must be substantially the same as that in compression if the wave formation occurs only in the close proximity of the most highly stressed compressive fiber, since then the stress is materially constant in the region involved. Critical stresses predicted by the theoretic formulas of the diamond pattern general instability were checked at the Guggenheim Aeronautics Laboratory of the California Institute of Technology (GALCIT).[4] It was found that the theoretic critical stress was invariably higher than the experimental stress, in some cases more than ten times as much.

Two reasons may be put forth in explanation of the discrepancy. First, it is likely that in most of the specimens tested at GALCIT the wave length in the circumferential direction was so large that the variation of the direct stress due to bending had a decisive influence upon both the distortion pattern and the critical stress. If this is true, the instability cannot be classified as of the "diamond pattern in compression" type and the critical stress has to be calculated as suggested in the last section of this paper. Second, in all the test specimens the wave formation was restricted to areas where the sheet covering buckled long before general instability occurred. Thus the resistance of the sheet to shear was materially reduced. It is conceivable that a modification of Dschou's or Taylor's theoretic formulas to take care of this effect would result in better agreement between theory and experiment.

One might be inclined to expect better agreement also with bent monocoque cylinders in which the sheet covering does not buckle before general instability occurs. This can be the case in cylinders of large radius reinforced with closely spaced weak stringers and rings. It is quite likely, however, that the "linearized" theory of elasticity does not suffice for the calculation of the critical stresses of such structures, since it is known from the investigations of von Kármán, Tsien, and Dunn[7] that a nonlinear theory is necessary to explain the discrepancy between theory and experiment in the case of the buckling of thin-walled nonreinforced cylinders.

Flattening in Bending

Brazier[1] showed that an isotropic thin-walled circular cylinder flattens to an elliptic shape when a pure bending moment is applied to it. The flattening increases gradually when the applied moment is increased, and the cylinder collapses when the moment reaches its critical value.

Brazier's calculations were extended by Heck[5] to describe the behavior of orthotropic cylinders of elliptic cross section and by the writer (Part 2)[6] to describe the behavior of circular cylindrical structures consisting of stringers, rings, and a very thin sheet covering. According to all these investigations, buckling occurs after the diameter of the cylinder foreshortens gradually to seven-ninths of its original length. This circumstance forcibly rules out the "flattening in bending" type of general instability as a form of buckling of actual aircraft structures. No designer or licensing authority is likely to consider an aircraft structure airworthy if its elastic distortions during actual flight attain such magnitude. On the other hand, in large airplanes it might be well to calculate, by the theoretic formulas of Part 2 of reference 6, the amount of flattening, in order to check whether the structure has adequate stiffness, and the stresses caused by flattening, in order to ascertain that the structure has adequate strength. The experiment reported by the writer[6] showed reasonable agreement with calculations.

Inward Bulge in Bending

Because of the lack of a better expression this name has been chosen to indicate that the characteristic feature of this type of buckling is an inward bulge that develops symmetrically to the most highly stressed fiber in compression (see Fig. 3). In some cases secondary bulges also appear and the deflected shape slightly resembles the diamond pattern in compression already described. However, deflections are greatest near the most highly stressed fiber in compression, they decrease in magnitude toward the neutral axis, and the tension

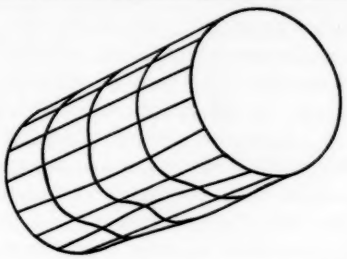

FIG. 3. Inward bulge type of general instability.

side of the cylinder remains smooth. This type of buckling was theoretically derived and in one single experiment was verified by the writer in 1937.[6] In the calculations the monocoque cylinder of circular cross section was assumed to consist of stringers, rings, and a very thin sheet covering. The buckling load was determined by the Rayleigh-Ritz-Timoshenko method, and the strain energy stored in the sheet covering was neglected.

Experimental results of an extensive series of investigations are available for checking the validity of the theory of the inward bulge type of buckling. These experiments were carried out at GALCIT as part of a research program undertaken to clarify the problems of general instability. Results were submitted to the Civil Aeronautics Authority in five reports between 1938 and 1940.[4] A summary of the investigations may also be found in Sechler and Dunn's textbook.[10] It appears that at buckling most of the specimens showed the inward bulge pattern. Nevertheless, a comparison at GALCIT of the test results with the writer's theoretic predictions showed marked disagreement. In the following sections of the present paper the assumption that caused the disagreement is discarded and the theory is amended accordingly. The revised theory yields simple formulas that show reasonable agreement with experiment.

Calculation of the Critical Load of the Inward Bulge Type of General Instability

The original calculations of the critical load of the inward bulge type of general instability were published by the writer in Part 3 of reference 6, where this type of instability was termed "local buckling of a monocoque structure." The calculations deal with a monocoque cylinder of circular cross section consisting of evenly spaced rings, evenly spaced stringers, and a very thin sheet covering. The cylinder is under the action of a constant bending moment applied at the end sections by means of loads distributed in conformity with the Bernoulli-Navier assumptions. It is further assumed that the structure distorts in accordance with the Bernoulli-Navier theory of bending until buckling occurs.

The stability of this state of equilibrium in bending is investigated by the Rayleigh-Ritz-Timoshenko method by determining the change in the total potential energy of the system during a virtual displacement. The displacement pattern is arbitrarily assumed to be that shown in Figs. 3, 4, and 5. It is given analytically

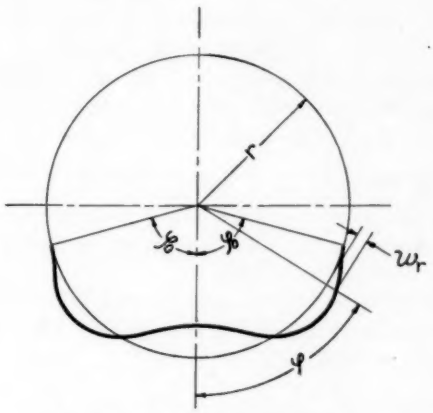

FIG. 4. Deflected shape of ring according to assumptions.

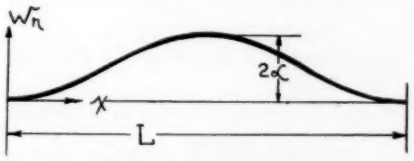

FIG. 5. Deflected shape of stringer according to assumptions.

by the expressions for the radial and tangential displacements w_r and w_t, respectively, of any point on the surface of the cylinder:

$$\left.\begin{aligned} w_r &= -(\alpha/2)[1 - \cos(2\pi x/L)][\cos(n\varphi) + \cos(2n\varphi)] \\ w_t &= (\alpha/2)[1 - \cos(2\pi x/L)][(1/n) \times \sin(n\varphi) + (1/2n)\sin(2n\varphi)] \end{aligned}\right\} \quad (1)$$

provided that

$$\varphi \leq \varphi_0 = \pi/n \quad (1a)$$

These equations satisfy a number of boundary conditions and represent inextensional deformations of the rings and stringers. They contain two arbitrary parameters—namely, L, which is the wave length in the longitudinal direction, and the number $n = \pi/\varphi_0$, which characterizes the wave length in the circumferential direction. Next, the strain energy due to the distortions according to Eqs. (1) is calculated, as well as the work done by the applied loads. The expressions obtained do not have terms with α; this circumstance indicates that the original undisturbed shape is a state of equilibrium (principle of virtual displacements). Whether or not this equilibrium is stable depends in the present case upon the terms containing α^2. The critical value of the bending moment is reached—that is, the change from stability to instability occurs—when the strain energy stored in the structure is equal

to the work done during the virtual displacement. From this condition the critical load is calculated:

$$P_{cr} = (\pi^2 E I_{str}/L^2)[4\pi M_3 + (1/\pi^3)(1/\gamma)M_2]/(M_1 + R_1) \quad (2)$$

where

$$\gamma = (r/L)^3(r/d)(E_{str}I_{str}/NE_rI_r) \quad (3)$$

and

$$I_{str} = I_{str_r} + (5/8)(1/n^2)I_{str_t} \quad (4)$$

Furthermore,

$$\left.\begin{aligned} M_1 &= \sin(\pi/n)\{1 - [1/(1-n^2)] + [1/2(1-4n^2)] - [1/(1-9n^2)] + [1/2(1-16n^2)]\} \\ M_2 &= 17n^3 - 10n + (2/n) \\ M_3 &= (1/n) \\ R_1 &= (1/2n^2)\sin(\pi/n)\{(5/4) - [1/(1-n^2)] - [1/(1-4n^2)] + [1/(1-9n^2)] - [1/4(1-16n^2)]\} \end{aligned}\right\} \quad (5)$$

In these equations

P_{cr} = the critical load of the most highly stressed stringer in compression
I_{str_r} = the moment of inertia of a stringer for radial bending
I_{str_t} = the moment of inertia of a stringer for tangential bending
I_r = the moment of inertia of a ring (for radial bending)
E_{str} = the modulus of the material of the stringer
E_r = the modulus of the material of a ring
L = the wave length in the longitudinal direction
r = the radius of the cylinder
d = the stringer spacing
N = a number dependent on the number m of rings that distort within one wave length during buckling

Values of N are given in a table[6] for $m = 1, 2, 3, 4,$ and 5.

With L_1 denoting the ring spacing one has

$$L = (m + 1)L_1 \quad (6)$$

The magnitude of the critical load given in Eq. (2) depends upon the two parameters n and $m = (L/L_1) - 1$. At buckling the parameters must have values that make P_{cr} a minimum. The critical load[6] is minimized in the following way: The differential coefficient of P_{cr} with respect to n is calculated and equated to zero, and between the equation so obtained and Eq. (2) γ is eliminated. The critical load may then be given in the form

$$P_{cr} = \pi^2 E_{str}I_{str}/(\lambda L_1)^2 \quad (7)$$

where λ is the equivalent length coefficient. The value of λ depends upon the number m of rings involved in buckling and upon a structural coefficient Λ given by the equation

$$\Lambda = (r^4/L_1{}^3d)(E_{str}I_{st}/E_rI_r) \quad (8)$$

The minimum value of P_{cr} with respect to $m = (L/L_1) - 1$ is then determined graphically with the aid of Fig. 19[6] in which the equivalent length coefficient λ is plotted against the structural coefficient Λ for different values of m. From this chart the buckling load of the most highly stressed stringer of any actual monocoque cylinder can be easily calculated. One has only to determine the structural coefficient Λ of the particular monocoque structure and take from the chart the corresponding highest value of λ compatible with the number m of the rings which can be involved in buckling.

A printing error in reference 6 should be pointed out here. The expression in the first parenthesis on the right-hand side of the last of Eqs. (5) of the present paper (Eq. 78·a[6]) was printed erroneously as "$^1/_2n^2$" instead of the correct "$1/2n^2$." Moreover, Eq. (87) of reference 6 was misinterpreted at GALCIT. Its right-hand side was originally printed as $[1/(m+1)^3 \cdot N_m]\Lambda$. It was read as $\{[1/(m+1)^3]N_m\}\Lambda$ instead of the correct $\{1/[(m+1)^3 N_m]\}\Lambda$.

Effect of the Sheet Covering

Reference 4 contains several diagrams and photographs showing the distortions after failure of the specimens tested at GALCIT. Some of the specimens displayed in the figures are of the regular sheet-covered monocoque type; others have wire bracings across the panels in place of the sheet covering. The distortions of the latter show good agreement with the assumptions stated in the preceding section. The former group includes some test pieces that failed definitely according to the inward bulge pattern; others, the buckling of which might possibly be classified as being of the diamond pattern type; and still others, in which the wave length in the longitudinal direction was equal to the ring spacing so that the buckling was clearly not of the general instability type.

Although the distortion pattern is not necessarily the same at incipient buckling and after failure has occurred, one might expect reasonably good agreement between theory and experiment in the value of the buckling load if the distortions measured after failure were similar to those assumed in the calculations. Nevertheless, at GALCIT the buckling loads obtained by experiment were from one and two-tenths to nine times greater than those calculated by the theory. The reason for this discrepancy may be found in the effect of the sheet covering and of the wire bracing in the two kinds of specimens.

The buckled shape given by Eqs. (1) corresponds to inextensional (purely bending) deformations of the rings and stringers. The same distortion pattern, however, involves shearing deformations of the covering which were disregarded in the theory when the sheet was assumed to be infinitely thin. If the covering is in the nonbuckled state, the strain energy due to the

shearing strain is many times greater than that due to the bending of the stringers and rings. On the other hand, the resistance to shearing deformations is extremely small in the panels that had buckled before the occurrence of general instability. Thus it is reasonable to assume that the inward bulge is restricted to portions of the cylinder where the panels of sheet covering are in the buckled condition. This statement, however, means that the wave length in the circumferential direction is determined by the condition of the panels of sheet and, consequently, must not be calculated from the minimum requirement stated in the preceding section. In this connection it is worth noting that the envelope of the curves of Fig. 19[6] corresponds to the deformations extending over the entire circumference ($n = 1$) and that the envelope contains the values of λ to be used if the monocoque cylinder is reasonably long.

The determination of the length of the arc of circumference involved in buckling is not yet possible without recourse to experiment. Among other things the length is influenced by the critical stress of the panels, by the maximum stress in the cylinder, and by the shift of the neutral axis of the cylinder due to the ineffectiveness of the buckled sheet in carrying compression. It is reasonable to assume, however, that $\varphi_0 = \pi/n$ is equal to, or smaller than, 90°.

Similar considerations may be offered in the case of the wire-braced specimens. On the tension side of the monocoque the crossed wires are under tension and prevent changes of the right angles subtended by stringers and rings. On the compression side, however, the wires slacken and permit small changes in the angles. The length of the arc of circle involved in the inward bulge type of buckling depends, therefore, upon the amount of distortion necessary for general instability as well as upon the initial tension in the wires. A purely theoretic calculation of these effects is not yet possible.

On the other hand, if the value of n is known, the formulas developed in the preceding section may be simplified considerably.

Revised Theory

If n is a known constant, the buckling load P_{cr} of the most highly stressed stringer is a function of the longitudinal wave length L only. In such a case every symbol in Eq. (2) is a constant except L and γ. These two can be expressed in terms of $(m + 1)$ if one makes use of Eqs. (3) and (6) and calculates the value of N in Eq. (3). N is the number by which the strain energy stored in a ring at the middle of the longitudinal wave length must be multiplied in order to obtain the total strain energy stored in the m rings within one wave length. The strain energy in any one ring is proportional to the square of the maximum deflection. The maximum deflection β of the ring in the middle of the wave is -2α as may be seen from the first of Eqs. (1).

The maximum deflection of the i^{th} ring is

$$\beta_i = -\alpha\{1 - \cos [2\pi i/(m + 1)]\} \tag{9}$$

Consequently,

$$N = (1/4)\sum_{i=1}^{i=m} \{1 - \cos [2\pi i/(m + 1)]\}^2 \tag{10}$$

It is shown in the Appendix that, by carrying out the summation indicated on the right-hand side of Eq. (10),

$$\left.\begin{aligned} &N = (3/8)\ (m + 1) \text{ if } m = 2, 3, 4, \ldots \\ &\text{By definition} \\ &N = 1 \text{ if } m = 1 \end{aligned}\right\} \tag{11}$$

With the aid of Eqs. (3), (6), and (11) Eq. (2) can be transformed:

$$P_{cr} = \frac{\pi^2 E_{str} I_{str}}{L_1^2} \frac{1}{(M_1 + R_1)} \left\{ \frac{4\pi M_3}{(m + 1)^2} + \frac{3}{8} \frac{M_2}{\pi^3} \frac{(m + 1)^2}{\Lambda} \right\} \tag{12}$$

In this equation E_{str} is the modulus for the material of the stringer, I_{str} is given in Eq. (4), L_1 is the distance between adjacent rings, Λ is the nondimensional structural coefficient given in Eq. (8), and the values of M_1, M_2, M_3, and R_1 can be computed from Eqs. (5). The critical load can be calculated, therefore, if the number m of the rings involved is known. In a long monocoque cylinder m will have the value that makes P_{cr} a minimum. Assuming arbitrarily that N is a continuous function of m and is represented by the first of Eqs. (11), the minimum value of P_{cr} can be determined by differentiating Eq. (12) with respect to m and equating to zero the differential coefficient. The equation so obtained can be solved for m:

$$m = (32/3)^{1/4}\, \pi (M_3/M_2)^{1/4} \Lambda^{1/4} - 1 \tag{13}$$

This is the number of rings that distort within one wave length when the buckling load is a minimum. Eq. (13) can be written in the form

$$m = \psi \Lambda^{1/4} - 1$$

In Fig. 6 computed values of m are plotted against $(1/n)$. The curve so obtained may be represented with an accuracy sufficient for practical purposes by the formula

$$\psi = (2.84/n)$$

Thus

$$m = (2.84/n)\Lambda^{1/4} - 1 \tag{14}$$

Eqs. (13) and (14) are approximate, since by definition m must be an integer. Nevertheless, substitution of the value of m from Eq. (13) into Eq. (12) should give the critical load P_{cr} sufficiently accurately if the number m of rings required for a minimum of P_{cr} is available.

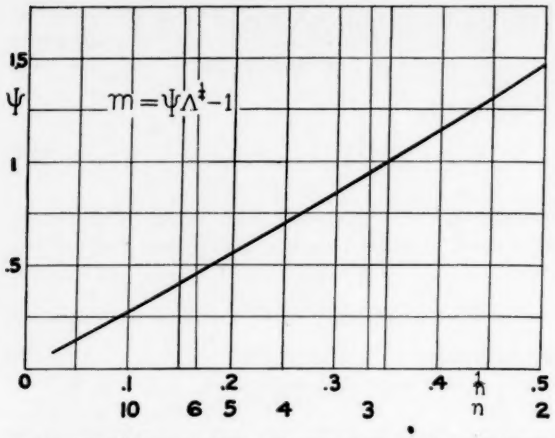

FIG. 6. Number m of rings in a wave when P_{cr} is a minimum.

$$P_{cr} = \pi^2 E_{str} I_{str} / (\lambda L_1)^2 \tag{15}$$

where the equivalent length coefficient λ has the value

$$\lambda = k\Lambda^{1/4} \tag{16}$$

and the coefficient k can be determined from the equation

$$k^2 = (\pi/\sqrt{6})[(M_1 + R_1)/\sqrt{M_2 M_3}] \tag{17}$$

In Fig. 7 computed values of k are plotted against $1/n$. It can be seen from Fig. 7 that a good approximate formula for k is

$$k = 1/n \tag{18}$$

With the aid of Eqs. (16) and (18) Eq. (15) may be rewritten in the form

$$P_{cr} = n^2 \pi^2 E_{str} I_{str} / L_1^2 \Lambda^{1/2} \tag{19}$$

Upon substitution of Λ from Eq. (8), Eq. (19) becomes

$$P_{cr} = n^2 \sqrt{\frac{d}{L_1}} \frac{\pi^2 \sqrt{E_{str} I_{str} E_r I_r}}{r^2} \tag{20}$$

According to Eq. (20) the maximum load that the most highly stressed stringer can carry is equal to the buckling load of a column, the length of which is equal to the radius of the cylinder and the bending rigidity of which is equal to the geometric mean of the bending rigidities of stringer and ring, provided that an end fixity factor $C = n^2\sqrt{d/L_1}$ is used. In the expression for the end fixity coefficient, (d/L_1) is the ratio of the stringer spacing to the ring spacing and $n = \pi/\varphi_0$. This formula may be given in several alternate forms if desired. One of them is

$$\epsilon_{cr} = n^2 \pi^2 (\rho_{str} \rho_r / r^2)(E_r t_r / E_{str} t_{str})^{1/2} \tag{21}$$

where ϵ_{cr} is the critical strain in the most highly stressed fiber of the monocoque cylinder and the other symbols not previously defined are given by the formulas

$$\left.\begin{aligned} \rho_{str}^2 &= I_{str}/A_{str} & \rho_r^2 &= I_r/A_r \\ t_{str} &= A_{str}/d & t_r &= A_r/L_1 \end{aligned}\right\} \tag{22}$$

A_{str} and A_r are the cross-sectional areas of a stringer and a ring, respectively, including the effective width of sheet.

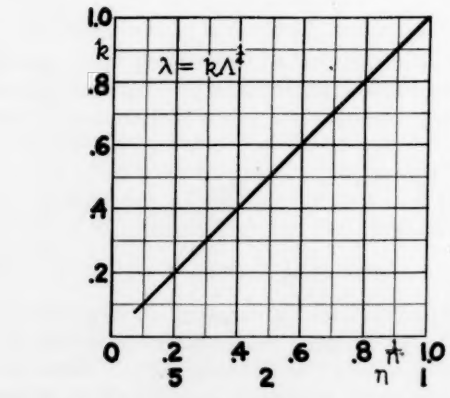

FIG. 7. Value of the equivalent length coefficient λ when P_{cr} is a minimum.

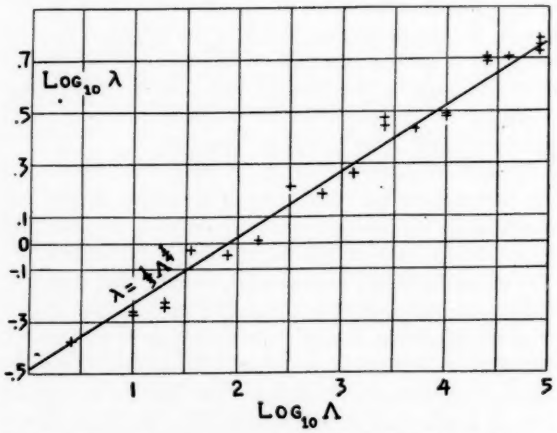

FIG. 8. Theoretic and experimental values of λ for wire-braced specimens ($n = 3$).

COMPARISON WITH EXPERIMENT

The formulas for the buckling load developed in the preceding section are easy to use if the wave length in the circumferential direction and, consequently, the value of n are known. For the time being this value has to be determined by experiment. An analysis of the 22 wire-braced test specimens of the GALCIT investigations yielded $n = 3$ as the best value. With this, $k = 1/3$ from Eq. (18) and Eq. (16) becomes

$$\lambda = (1/3)\Lambda^{1/4} \tag{23}$$

A graphic representation of this formula on logarithmic paper is a straight line with a slope equal to one-fourth. It is shown in Fig. 8. The figure also contains values computed from the GALCIT experiments. The abscissa of each experimental point was calculated from Eq. (8); the ordinate, from Eq. (15) in which the

experimentally determined value was substituted for P_{cr} and the equation was then solved for λ.

The experimental points are in fair agreement with the theoretic straight line. The maximum deviation to the safe side is 20 per cent; the average deviation, 10 per cent. The maximum deviation to the unsafe side is 26 per cent; the average deviation, 12.5 per cent.

In Fig. 9 theory and experiment are compared on the basis of the 35 sheet-covered GALCIT test specimens that failed in general instability. The value of n is again assumed to be 3. With sheet-covered speci-

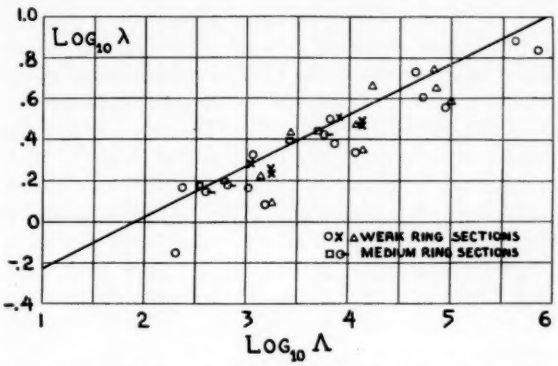

FIG. 9. Theoretic and experimental values of λ for sheet-covered specimens ($n = 3$).

mens the radial and tangential moments of inertia must be calculated with proper consideration of the effective width of sheet, and the difference between the location of the centroid of the section plus effective width and that of the centroid of the section alone must not be neglected. In the case of the stringers Marguerre's cube root formula was used for the effective width of the flat sheet, and the influence of the curvature was taken into account according to Ebner's suggestion. The maximum stress measured in the tests was taken for the edge stress. The pertinent formulas are discussed in Part 1 of reference 6. They are given below in a slightly modified form and with the notation of the present paper.

$$2w' = 2w + (\epsilon_{\text{curved}}/\epsilon_{max.})(d - 2w) \tag{24a}$$

$$2w = [\epsilon_{\text{flat}}/(\epsilon_{max.} - \epsilon_{\text{curved}})]^{1/3} d \tag{24b}$$

$$\epsilon_{\text{flat}} = 3.62(t/d)^2 \tag{24c}$$

$$\epsilon_{\text{curved}} = 0.3(t/r) \tag{24d}$$

In the above formulas $2w'$ is the effective width of the curved sheet; $\epsilon_{max.}$ the strain measured in the most highly stressed stringer on the compression side of the test specimen; d, the stringer spacing; t, the thickness of the sheet metal covering; and r, the radius of the cylinder. In the case of the rings the effective width of sheet is assumed to be equal to the width of the ring section for reasons discussed in paragraph 22.[6] Except for the above details, the procedure in calculating the experimental points is the same in Figs. 8 and 9.

The experimental points of Fig. 9 show the general trend of the theoretic straight line, but the scattering is considerable. The maximum deviation to the unsafe side is 19 per cent; to the safe side, 44 per cent. The average deviation to the unsafe side is 7 per cent; to the safe side, 22 per cent. According to these figures some of the specimens failed under much higher loads than those predicted by theory on the assumption of $n = 3$, since in the equation of the critical load the value of λ appears to the second power.

In order to get an insight into the reasons for the discrepancy, the values of n that make theory and experiment agree were calculated for each specimen. Since n enters into the calculation of I_{str} (see Eq. 4), it was necessary to proceed in the following way:

Using subscripts 3 and p to indicate that n is assumed to have the value 3 and p, respectively, Eq. (3) may be rewritten in the form:

$$P_{cr} = \pi^2 E_{str} I_{str_3}/(\lambda_3 L_1)^2$$

Substituting for P_{cr} the value $P_{exp.}$ obtained in experiment,

$$\lambda_3 = [\pi^2 E_{str} I_{str_3}/P_{exp.} L_1^2]^{1/2} \tag{25}$$

This is the experimental value of λ provided that $n = 3$. If $n = p$,

$$\lambda_p = [\pi^2 E_{str} I_{str_p}/P_{exp.} L_1^2]^{1/2}$$

Consequently,

$$\lambda_p = \lambda_3 [I_{str_p}/I_{str_3}]^{1/2}$$

Moreover, from Eq. (8)

$$\Lambda_p = \Lambda_3 (I_{str_p}/I_{str_3})$$

According to Eqs. (16) and (18), theory requires that

$$\lambda = (1/n)\Lambda^{1/4}$$

Thus

$$\Lambda_p = p^4 \lambda_p^4$$

Substituting the above determined values,

$$\Lambda_3 = p^4 \lambda_3^4 [I_{str_p}/I_{str_3}]$$

Substituting for I_{str_p} its value from Eq. (4) and transforming the expression so obtained,

$$p^4 I_{str_r} + p^2 (5/8) I_{str_t} - (\Lambda_3 I_{str_3}/\lambda_3^4) = 0 \tag{26}$$

This is a quadratic in p^2. I_{str_r} and I_{str_t} are properties of the stringer section, I_3 and Λ_3 can be calculated from Eqs. (4) and (8) with $n = 3$, and λ_3 is the "experimental" coefficient calculated from Eq. (25). Solution of Eq. (26) for p gives the value of n that makes Eq. (16) hold.

For every sheet-covered specimen the value of n was determined according to the above outlined procedure. It was found that n varied between 2.12 and 5.59. A qualitative explanation for the differences in the values of n is not difficult to find. The inward bulge can de-

velop only if the distortions of the stringers and rings are not restrained materially by the panels of sheet. However, the resistance of the sheet to distortions depends upon two circumstances: first, whether it is in the buckled state and, second, how much movability results from its buckling.

The length of the arc of the circumference along which the panels had buckled depends upon the ratio of the stress in the most highly stressed fiber of the cylinder to the buckling stress of a panel of sheet. Since in most cases the curvature effect is decisive, the buckling stress of the panel may be assumed to be proportional to Et/r, where E is the modulus of the material, t is the thickness of the sheet, and r is the radius of the cylinder. Thus the ratio of the greatest stress to the buckling stress is proportional to $\epsilon_{max.} r/t$, where $\epsilon_{max.}$ is the greatest strain measured in the experiment. This quantity is one of the parameters that may be expected to have influence upon the value of n.

The amount of movability resulting from buckling depends upon the ratio of the difference between the length of the arc of the panel and the length of its chord to the length of the chord. In a first approximation this ratio is equal to r/d, as can be proved without difficulty. Consequently, r/d is the second parameter in question.

In Fig. 10 calculated values of n are plotted against the two parameters $(\epsilon_{max.} r/t)$ and (r/d). Curves of constant n are drawn in a way to give the best agreement with experiment. The figure shows that n is large if $\epsilon_{max.} r/t$ is small—that is, if the sheet had buckled along only a small part of the circumference—and if r/d is large—that is, if buckling caused only a small amount of movability. Moreover the effect of $\epsilon_{max.} r/t$ upon n is small if r/d is small—that is, if the movability of the buckled panels is great—and the effect of r/d upon n is small if $\epsilon_{max.} r/t$ is large—that is, if the buckling stress is well exceeded in many panels of sheet.

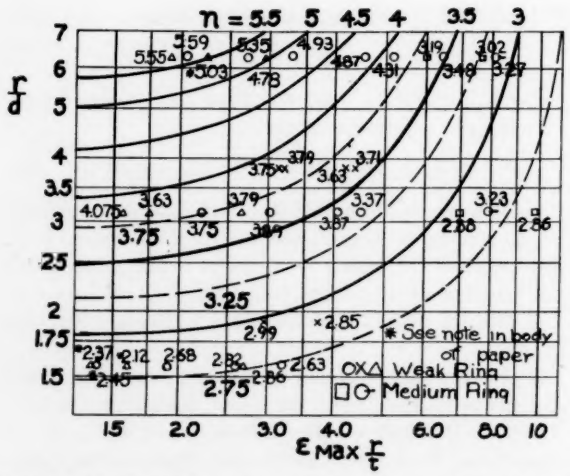

FIG. 10. Experimental values of n for sheet-covered specimens.

It may be seen from Fig. 10 that the differences are small between the values of n according to the curves and according to the experimental points. The maximum difference is 14 per cent and the average difference is 4.4 per cent, if one does not include the four points for which n is equal to 5.03, 2.45, 2.37, and 2.12. With the first two, failures started by panel instability; with the last two, a consistent application of the formulas resulted in an exaggerated increase in the value of the moment of inertia due to the effective width of sheet. In the case of the last two points the differences are: 18 per cent for point 2.37 and 29 per cent for point 2.12.

In all the above calculations it was assumed that the test cylinders were long enough to develop the distortion pattern corresponding to the minimum value of the critical load. The validity of this assumption was checked with the aid of Eq. (14). It was found that the number m of rings required for a minimum of the critical load was available in all but the specimens plotted at the lower left corner of Fig. 10. A recalculation of the critical load of these specimens with the aid of Eq. (12) was not carried out, since the accuracy of the computed critical loads of these specimens is doubtful for the reason discussed under paragraph 5 in the following section.

VALIDITY OF THE CALCULATIONS

The validity of a theoretic calculation depends upon the assumptions made. In a discussion of the validity of the present calculations the following items must be considered:

(1) Assumption of inextensional deformations.
(2) Assumptions concerning the distortion pattern.
(3) Assumptions concerning the circumferential wave length.
(4) Method of calculating the buckling stress of a curved panel.
(5) Method of calculating the effective width.
(6) Assumption of the same moment of inertia for each stringer.
(7) Assumption of the validity of Hooke's law.
(8) A disregard of the shift of the neutral axis.

A discussion of these items follows.

(1) It is believed that the assumption of inextensional deformations of stringers and rings is satisfactory if the panels of sheet covering buckle well before general instability occurs. In such a case the strain energy stored in the sheet due to the inward bulge type of instability is negligibly small, and the strain energy stored in the stringers and rings is a minimum for inextensional distortions. If, however, general instability occurs before the buckling of the panels, the strain energy stored in the three elements—namely, stringer, ring, and sheet—is likely to be a minimum for a distortion pattern in which the distortions of stringers and rings are not inextensional. The present theory does not include this type of general instability, the calculation

of which would probably require the development of a nonlinear theory of the orthotropic cylinder along the lines of reference 7.

(2) It would be possible to make the assumptions concerning the distorted shape of the rings conform better with experiment by adopting a new expression for the distortions containing several parameters. It is likely, however, that the deviations of the present assumptions from the true deflected form have a smaller influence upon the critical loads than do the other items discussed below. Thus a revision of the assumptions concerning deflections does not appear warranted before the other more important questions are clarified.

(3) Because of the inaccuracy of the assumptions concerning the distortions near the boundary of the bulge ($\varphi = \varphi_0$) the value of n has no real physical significance. The angle $\varphi_0 = \pi/n$ approximately represents the limit of the major distortions and thus roughly coincides with the angle beyond which the panels of sheet are in the buckled state or beyond which the wire bracing is slack. The actual value of n, however, must be determined from experiment. It was found to be approximately 3 for the wire-braced specimens and to vary considerably in the case of the sheet-covered specimens, as shown in Fig. 10.

(4) The buckling stress of the curved panels of sheet is of importance in the calculation of the effective width, which in turn influences materially the value of the critical load in general instability. Unfortunately, the actual value of the numerical coefficient in Eq. (24c) is not necessarily 0.3, and it may even vary from specimen to specimen. However, because of the uncertainty of the basis of the theory of buckling of thin curved sheets and in view of the not clearly defined edge conditions, a refinement of the calculations involving the use of different coefficients in different specimens does not seem to be warranted.

(5) The calculation of the effective width of sheet with the aid of Eqs. (24a) and (24b) is not reliable, but no better method is known to the writer. General practice is followed in the use of the effective width so obtained in the calculation of the radial moment of inertia of the stringer plus effective width combinations. On the other hand, the adoption of the same effective width for the calculation of the tangential moment of inertia was entirely arbitrary. This circumstance is believed to have led to exaggerated values of I_{str} and, consequently, to too low values of n in the case of the specimens marked 2.37, 2.12, 2.68, 2.82, 2.86, and 2.63 in Fig. 10.

From a theoretic standpoint the reduced effective width should be used in the calculations instead of the effective width. This means that in Eq. (24b) the right-hand side should be multiplied by two-thirds. The factor was omitted, since the average effective width over all the stringers involved in general instability is greater than the effective width of the most highly stressed stringer, as discussed under (6).

(6) In the derivations it was assumed that the moment of inertia I_{str} was the same for every stringer involved in buckling. In reality this moment of inertia varies with the location of the stringer. Thus some average value should be used rather than the minimum corresponding to the most highly stressed stringer, but in what way this average should be calculated is unknown. The procedure of calculating I_{str} for the most highly stressed stringer was adopted for two reasons: first, it gives a clearly defined rule for the computations and, second, the most highly stressed stringer contributes the greatest amount to the expressions in the energy calculations.

(7) It was assumed that Hooke's law was valid for all the elements involved. In some of the test pieces the maximum strain $\epsilon_{max.}$ was above the proportional limit. Since the stress-strain curve of the material was not known, it was impossible to determine accurately the effect of exceeding the proportional limit. It is not likely, however, that this circumstance would appreciably influence the results.

(8) The neutral plane of the bent cylinder was assumed to be the plane of symmetry of the unloaded cylinder. This is not true when part of the sheet covering is ineffective due to buckling, but this circumstance is not likely to influence appreciably the results.

The above discussed shortcomings of the theory are balanced by the use of a value n calculated from experiment. Thus it is reasonable to believe that the critical load in the inward bulge type of instability of monocoque cylinders having proportions similar to the GALCIT test specimens can be predicted with an accuracy sufficient for practical purposes if the procedure outlined in the next section is followed. For monocoque cylinders that differ materially from the GALCIT specimens no such definite statement can be made without further tests. In many practical cases, however, a reasonable amount of agreement may be expected, since the present procedure seems to work for such dissimilar structures as the wire-braced cylinders and the sheet-covered monocoques having rings of small cross section.

If some of the above-listed assumptions were replaced by different ones, the curves of Fig. 10 would have to be modified. For instance, a change in the calculation of the tangential moment of inertia would materially alter the curves in the lower left corner but would influence the rest of the figure only slightly. It is hoped that future investigations will succeed in establishing a more rational basis for the determination of the coefficient n.

From a comparison of the formula developed in the present paper with the empirical GALCIT formula of page 333, reference 10, the following conclusions may be drawn:

The GALCIT formula gives excellent agreement in the case of the test specimens that have the smallest ring section. In these the ratio of the moment of inertia of the stringer to that of the ring is 24.3 if the effective

width of the sheet is disregarded. For the calculation of the instability of these test pieces the GALCIT formula is superior to the formula of the present paper.

In the case of the five test specimens having the two heavier ring sections the ratio is 1.36 and 1.20. With these the agreement of the GALCIT formula is not quite so good. Critical loads calculated by it are just about as close to the experimental values as those calculated by the formula of the present paper. This is true if the curves of reference 4 are considered; in Fig. 8·13 of reference 10 two of the points are replotted on the assumption of a reduced effective radius of gyration. Theory does not appear to give a reason for such a reduction, since the rings are not likely to be under the action of high compressive stresses before general instability occurs. Nevertheless, the reduction would be perfectly acceptable if supported by sufficient experimental evidence. This, however, is not yet available.

In the case of the wire-braced specimens the GALCIT formula fails to give agreement with experiment. Sechler and Dunn do not suggest its use for this type of structure, and the experimental points are not included in Fig. 8.13 of reference 10. On the other hand, the formula of the present paper leads to reasonable agreement with experiment in the case of the wire-braced specimens. Consequently, the predicted critical load of a monocoque cylinder in which the moment of inertia of a ring is greater than the moment of inertia of a stringer should be regarded with greater caution if calculated by the GALCIT formula than if calculated by the procedure of the present paper.

Procedure Suggested for the Calculation of the Critical Stress of the Inward Bulge Type of Instability in Pure Bending

(1) Assume the value of the critical strain $\epsilon_{max.}$

(2) Calculate the effective width $2w'$ of the sheet by Eqs. (24).

(3) Determine the moments of inertia of the stringer plus effective width for bending in the radial direction (I_{str_r}) and in the tangential direction (I_{str_t}). Calculate (I_{str}) with the aid of Eq. (4). Assume $n = 3$ if no more accurate value is available.

(4) Calculate the moment of inertia I_r of the ring, assuming that the effective width of sheet is equal to the width of the ring.

(5) Calculate the critical load P_{cr} of the most highly stressed stringer from Eq. (20), assuming $n = 3$ if no more accurate value is available. The maximum compressive stress is then P_{cr}/A_{str}, where A_{str} is the cross-sectional area of the stringer plus the effective width of sheet and $\epsilon_{max.}$ is the maximum stress divided by E.

(6) If $\epsilon_{max.}$ calculated according to (5) differs greatly from its value assumed under (1) and if the corresponding value of n in Fig. 10 differs greatly from its value assumed under (3) and (5), repeat the procedure with new assumptions for $\epsilon_{max.}$ and n until satisfactory agreement is reached.

Eq. (14) may be used for ascertaining that the number m of rings that distort within one wave length, when P_{cr} is a minimum, is not greater than the number of rings available. If it is greater, Eq. (12) should be used for calculating the critical load, and the number of rings available should be substituted for m. It should be noted, however, that the use of Eq. (20) instead of Eq. (12) causes an error on the safe side.

If the moment of inertia of the ring is equal to, or greater than, the moment of inertia of the stringer and if the sheet covering is thin, the assumption of $n = 3$ is likely to give a reasonable approximation. With this assumption Eq. (20) becomes

$$P_{cr} = 88.83\sqrt{\frac{d}{L_1}}\,\frac{\sqrt{E_{str}I_{str}E_rI_r}}{r^2} \tag{27}$$

where

$$I_{str} = I_{str_r} + 0.06944I_{str_t} \tag{28}$$

Acknowledgment

The writer is indebted to Eugene S. Davidson for the analysis of the experimental data and the comparison with theory. This work was continued by Conrad Crown, who also made theoretic calculations, in particular those contained in the Appendix.

Appendix

The summation indicated in Eq. (10) can be carried out in the following way:

$$N = \frac{1}{4}\sum_{i=1}^{m}\left[1 - \cos\frac{2\pi i}{m+1}\right]^2$$

$$= \frac{1}{4}\sum_{i=1}^{m}\left[1 - 2\cos\frac{2\pi i}{m+1} + (1/2)\left(1 + \cos\frac{4\pi i}{m+1}\right)\right]$$

$$= (3/8)m - \frac{1}{2}\sum_{i=1}^{m}\cos\frac{2\pi i}{m+1} + \frac{1}{8}\sum_{i=1}^{m}\cos\frac{4\pi i}{m+1}$$

The above two sums can be calculated if the following transformation is considered:

$$F = \cos y + \cos 2y + \cos 3y + \ldots + \cos(n-1)y + \cos ny =$$

$$[1/(2\sin y)][2\sin y\cos y + 2\sin y\cos 2y + 2\sin y\cos 3y + \ldots + 2\sin y\cos(n-1)y + 2\sin y\cos ny]$$

With

$$2\sin A\cos B = \sin(A+B) + \sin(A-B)$$

the following formula is obtained:

$$F = [1/(2\sin y)][\sin 2y + \sin 3y - \sin y + \sin 4y - \sin 2y + \ldots + \sin ny - \sin(n-2)y + \sin(n+1)y - \sin(n-1)y]$$

In the brackets all but three terms cancel out. Thus

(*Continued on page 130*)

A Tabular Method of Propeller Blade Stress Analysis

JOSEPH STUART, III*
General Motors Corporation

SUMMARY

A tabular, trial-and-error method of evaluating the steady bending stresses in a rotating propeller blade is developed and examples of its application are given. The bending moment at a shank section of the blade is estimated and, by tabular integration, the corresponding radial bending moment distribution is calculated. Additional trials with appropriately revised shank section bending moment estimates are made until the correct distribution is found, having the physically required moment value of zero at the blade tip.

Tilted blades and blades whose section centers of gravity do not in general fall on the blade axis are shown to be readily analyzed. Because the final analysis can be quickly checked on a calculating machine and because the method is easily learned, versatile, and fast, its general adoption by the propeller industry is advocated.

SYMBOLS

- R = propeller tip radius, in.
- r = radial distance to blade section from propeller axis of rotation, in.
- z = distance a point is forward of a reference plane perpendicular to the propeller axis of rotation, in.
- Z = distance blade section c.g. is forward of the blade axis, in.
- T = thrust per blade, lbs.
- S = thrust shear acting, lbs. $(= -\int_r^R dT)$
- C.F. = centrifugal force acting through the blade section, lbs.
- M = net bending moment about section c.g., in.lbs.
- I = moment of inertia of blade section about line passing through section c.g. and parallel to the chord, in.[4]
- A = blade material cross-sectional area, sq.in.
- E = modulus of elasticity of blade material, lbs. per sq.in.
- X = radial distance separating two adjacent moment or two adjacent slope stations, in.

INTRODUCTION

THE IMPORTANT STEADY STRESSES in a rotating propeller blade are: (1) the direct tensile stress due to centrifugal force, and (2) the bending stress resulting from the net bending moment acting.

The centrifugal stress (= C.F./A) is readily evaluated. The bending stress is readily evaluated when the net bending moment is known.

DEVELOPMENT OF EQUATIONS

Fig. 1 shows schematically a portion of a rotating propeller blade. As is customary in propeller blade stress analyses, the blade has been untwisted, set at zero angle, and loaded with a thrust loading only.[1] The blade length has been divided by primary, numbered, moment stations into intervals X in. in length. The secondary, lettered, slope stations, also X in. apart, fall at the midpoints of the moment station intervals. Signs follow the conventions given in Niles and Newell.[2]

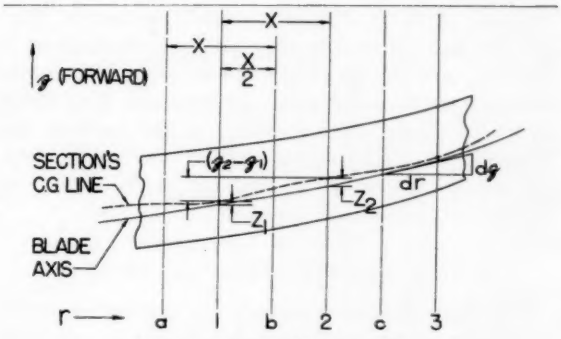

FIG. 1. Propeller blade portion.

Slope, dz/dr, values always refer to the blade axis and never to the line passing through the blade section c.g.'s. The fundamental expressions for this stress analysis method are developed from elementary beam theory as follows:

$$\int_{r_a}^{r_b} (M/EI)\, dr + (dz/dr)_a = (dz/dr)_b \qquad (1)$$

or, closely,

$$X(M/EI)_1 + (dz/dr)_a = (dz/dr)_b \qquad (2)$$

Eq. (2) gives an adequately accurate value for the axis slope at b in terms of the axis slope at a and the bending moment at 1, the midpoint of the slope stations' interval. For future convenience, Eq. (2) is multiplied through by X and rearranged to give:

$$[X^2/(EI)_1]M_1 + X(dz/dr)_a = X(dz/dr)_b \qquad (3)$$

The expression for the c.g. offsets of the running propeller is:

$$\int_{r_1}^{r_2} (dz/dr)\, dr + (Z_2 - Z_1) = (z_2 - z_1) \qquad (4)$$

or, adequately closely,

$$X(dz/dr)_b + (Z_2 - Z_1) = (z_2 - z_1) \qquad (5)$$

Presented at the Power Plants and Propellers Session, Eleventh Annual Meeting, I.Ae.S., New York, January 25-29, 1943.

* Technical Research Engineer, Aeroproducts Division.

In Fig. 1, Z_2 and Z_1 are, of course, exaggerated. The expression for the moment is found to be:

$$\int_{z_1}^{z_2} \text{C.F.}\, dz + \int_{r_1}^{r_2} S\, dr + M_1 = M_2 \qquad (6)$$

or, closely,

$$(z_2 - z_1)(\text{C.F.})_b + XS_b + M_1 = M_2 \qquad (7)$$

The first term in Eq. (7) is the centrifugal restoring moment increment.

As, EI, C.F., S, Z, and X values are known, Eqs. (3), (5), and (7) used in sequence give the slope at b, $(dz/dr)_b$, and the bending moment at 2, M_2, corresponding to the initial values $(dz/dr)_a$ and M_1. These equations permit the calculation of the moment distribution of a blade from an assumed root station bending moment value and known root slope, station by station out to the tip of the blade.

Tabular Application of Equations

The equations just developed lend themselves readily to tabular calculations. Fig. 2(A) shows the propeller blade selected for the examples, under static conditions. Its axis is then a straight line inclined forward at the tilt angle θ. The primary moment stations are designated by the solid transverse lines at 6-in. intervals, beginning with the 9-in. station and concluding at the 69-in. station, the tip station. The secondary slope stations are designated by the light, dashed transverse lines through the midpoints of the moment station intervals.

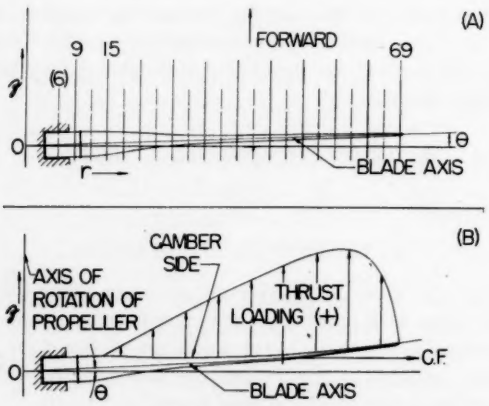

Fig. 2. Example propeller blade.

Fig. 2(B) shows the same propeller blade rotating. Its axis is curved forward and its slope is now equal to θ only at the constrained shank section. The normal, positive thrust loading shown gives negative, thrust shear (S) values, and positive bending moments, tending to place the camber side of the blade in compression. The centrifugal force, shear, I, and Z values of the example blade are plotted in Fig. 3. These values are

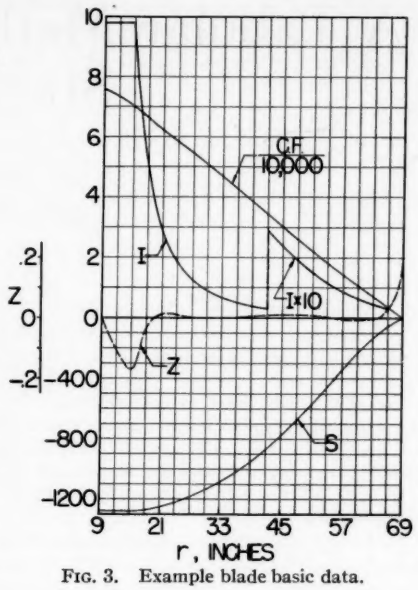

Fig. 3. Example blade basic data.

assumed to have been previously obtained by known methods.

Table 1 gives the final balanced trial for the example blade, for $X = 6$ in., $E = 29{,}000{,}000$ and $\theta = 0.3°$ or 0.005233 rad. at the constrained, 6-in., initial slope station. In Table 1 values from Fig. 3 are multiplied or subtracted, as indicated, to give columns 3, 6, 8, and 10 directly.

The initial entry in Table 1 is the known slope entry underlined at the head of column 5:

$$6 \times 0.005233 = \underline{0.03140.}$$

The other underlined entry is the 9-in., initial moment station, assumed root moment value of 28,032 in.lbs. From these starting values and the given values in columns 3, 6, 8, and 10, Eqs. (3), (5), and (7) are applied in sequence as follows:

$$0.00355 + \underline{0.03140} = 0.03495$$

These initial entries in columns 4 and 5 are in accordance with Eq. (3).

$$0.03495 + (-0.169) = -0.13405$$

These entries in columns 5, 6, and 7 are in accordance with Eq. (5).

$$(-9{,}920) + (-7{,}680) + 28{,}032 = 10{,}432$$

These entries in columns 9, 10, and 2 are in accordance with Eq. (7).

These sequences are repeated station by station out to the tip moment station. In this particular example the tip moment has the physically required value of zero and the bending moments listed in column 2 define the actual blade bending moment distribution.

Table 2 gives an adequately balanced moment distribution for the same blade analyzed in Table 1 save

TABLE 1

(1) Station	(2) M, In.Lbs.	(3) $\frac{36}{EI} \times 10^6$	(4) $\frac{36M}{EI}$	(5) $6\left(\frac{dz}{dr}\right)$	(6) $Z_2 - Z_1$	(7) $z_2 - z_1$	(8) C.F., Lbs.	(9) $(z_2 - z_1) \times$ C.F.	(10) $6S$
(6)				0.03140					
9	28,032	0.1267	0.00355						
(12)				0.03495	−0.169	−0.13405	74,000	−9,920	−7,680
15	10,432	0.1267	0.00132						
(18)				0.03627	+0.182	0.21827	65,700	14,340	−7,630
21	17,142	0.4320	0.00741						
(24)				0.04368	−0.013	0.03068	58,300	1,789	−7,330
27	11,601	0.9930	0.01152						
(30)				0.05520	0	0.05520	50,800	2,804	−6,860
33	7,545	1.855	0.01400						
(36)				0.06290	+0.006	0.07520	42,700	3,211	−6,140
39	4,616	3.268	0.01509						
(42)				0.08429	+0.004	0.08829	34,300	3,028	−5,200
45	2,444	5.214	0.01274						
(48)				0.09703	−0.003	0.09403	26,000	2,445	−4,085
51	804	8.271	0.00665						
(54)				0.10368	−0.012	0.09168	18,000	1,650	−2,790
57	−336	14.43	−0.00485						
(60)				0.09883	+0.001	0.09983	10,600	1,058	−1,375
63	−653	27.58	−0.01801						
(66)				0.08082	+0.213	0.29382	3,400	999	−346
69	0								

that the blade section c.g.'s are now considered to lie along the blade axis ($Z = 0$) and the root tilt value has been taken to be zero. Comparison with Table 1 indicates that for blades without c.g. offsets two columns fewer are required. The facility with which a new blade tilt can be analyzed is worthy of note.

For smaller blades or blades having large, erratic c.g. position shifts it may be desirable to take X equal to 3 in. rather than equal to 6 in. The basic equations indicate that in Table 1, "9" would replace "36" in the headings of columns 3 and 4 and "3" would replace "6" in the headings of columns 5 and 10. The stations would read (7.5), 9, (10.5), 12, etc.

These changes and their corresponding entry changes are the only complications entailed in changing X. However, to facilitate checking, it is recommended that X values of 6 or 3 in. be considered preferred values.

To facilitate checking it is desirable that final trials be run on a calculating machine. The last significant figure should be carefully rounded off to permit identical figures to be calculated by the checker.

TABLE 2

(1) Station	(2) M, In.Lbs.	(3) $\frac{36}{EI} \times 10^6$	(4) $\frac{36M}{EI}$	(5) $6\left(\frac{dz}{dr}\right)$ $(z_2 - z_1)$	(6) C.F., Lbs.	(7) $(z_2 - z_1) \times$ C.F.	(8) $6S$
(6)				0			
9	35,880	0.1267	0.00455				
(12)				0.00455	74,000	337	−7,680
15	28,537	0.1267	0.00362				
(18)				0.00817	65,700	537	−7,630
21	21,444	0.4320	0.00926				
(24)				0.01743	58,300	1,016	−7,330
27	15,130	0.9930	0.01502				
(30)				0.03425	50,800	1,648	−6,860
33	9,918	1.855	0.01840				
(36)				0.05085	42,700	2,171	−6,140
39	5,949	3.268	0.01944				
(42)				0.07029	34,300	2,411	−5,200
45	3,160	5.214	0.01648				
(48)				0.08677	26,000	2,256	−4,085
51	1,331	8.271	0.01101				
(54)				0.09778	18,000	1,760	−2,790
57	301	14.43	0.00434				
(60)				0.10212	10,600	1,082	−1,375
63	8	27.58	0.00022				
(66)				0.10234	3,400	348	−346
69	10						

ESTIMATION OF TRIAL ROOT MOMENTS

Usually only three trials are required to achieve a satisfactorily balanced moment distribution if the trial root moments are estimated as follows:

(1) Take the first trial root moment estimate equal to 70 per cent of the moment the thrust would cause if it acted upon a stationary blade.

(2) Take the second trial root moment estimate equal to the first estimate minus one-fourth of the tip moment found on the first trial.

(3) Linearly interpolate, or extrapolate, results of the first and second trials, accurately, to estimate the root moment for the third trial.

Fig. 4 shows a plot of tip moments against assumed root moments for the case considered in Table 1. The exact linearity displayed makes possible accurate interpolation over great ranges. The origin of the one-fourth rule is evident in the indicated slope of this particular curve.

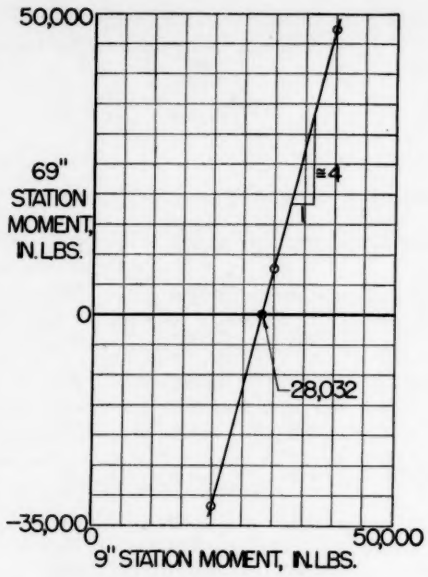

FIG. 4. Calculated tip moment versus assumed root moment.

That only roughly one-fourth of an applied tip moment would appear at the blade root seems reasonable enough when one reflects that the application of the moment would cause deflections generating neutralizing restoring moments.

SMALL UNBALANCED TIP MOMENTS

It will be noted that Table 2 was not perfectly adjusted but that an unbalanced tip moment of 10 in.lbs. was allowed to remain. Fig. 5 shows the bending stress distributions calculated for another propeller blade with substantially larger unbalanced tip moments. From Fig. 5 it is concluded that small residual tip moments have no important effect upon stress values determined for the highly stressed portions of the propeller blade. It is recommended that moment distributions for propeller blades, 10 ft. in diameter or larger, be considered adequately balanced when the residual tip moment is less than 50 in.lbs.

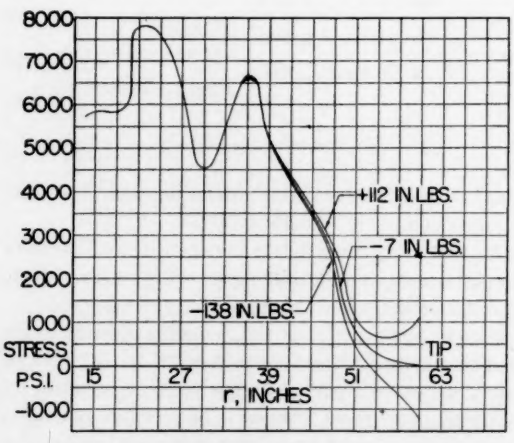

FIG. 5. Effect of unbalanced tip moments on blade bending stresses.

The above-noted insensitiveness of the blade bending stresses to small residual tip moments justifies the occasionally convenient practice of letting the final tip moment station fall as much as an inch beyond or an inch short of the actual tip of the blade.

As a direct check of the method described, moment distributions were tabularly determined for a representative propeller blade under the following operating conditions:

(1) Zero root tilt, take-off static thrust.

(2) 0.5 degrees root tilt, take-off static thrust.

(3) 0.5 degrees root tilt, windmilling at take-off r.p.m., with 10 per cent of maximum static thrust applied as negative thrust.

The tabularly determined moment distribution values were used as a basis for graphically determining deflections and corresponding centrifugal restoring and check net bending moment values. A comparison of the check and tabular distributions indicated that the greatest stress calculation error that would be encountered using the tabular method would be no greater than 250 lbs. per sq.in.—i.e., less than 1 per cent of the total steady stresses.

As a check of the minimum number of moment stations that it is safe to employ, the case given in Table 2 was analyzed using 21-, 7-, 6-, 5-, and 4-moment stations in addition to Table 2's 11-moment station analysis. Agreement between the distributions was entirely satisfactory for the 7-, 11-, and 21-moment station analyses.

Corrected root bending moments checked, for all moment station numbers, to within 0.5 per cent. Tip moments checked less well, however, when fewer than 7 stations were used. It is recommended that no fewer than 10-moment stations be used in final analyses.

ADVANTAGES AND RECOMMENDATION

In the two years that modifications of the method presented have been in use, three primary advantages have become evident:

(1) The simple, repeated, tabular calculation sequences are readily learned.

(2) The numerically recorded tabular calculations are quickly checked on a calculating machine.

(3) The method is several times faster than previous graphical methods.

It is hoped that the method presented is sufficiently versatile and offers enough real advantages to warrant its early general adoption by the aircraft propeller industry.

REFERENCES

[1] Weick, F. E., *Aircraft Propeller Design*, first Edition, p. 234; McGraw-Hill Book Company, New York, 1930.

[2] Niles, A. S., and Newell, J. S., *Airplane Structures*, second Edition, Vol. 1, p. 44; John Wiley & Sons, New York, 1938.

General Equations for the Analysis of Elliptical Rings*

DANIEL O. DOMMASCH†

Civil Aeronautics Administration

ABSTRACT

The analysis of bulkhead rings is at best a tedious process, and it is felt that any simplifications will be of help to the aircraft structural engineer.

Of the several methods of analysis available, that outlined in reference 1 seems to be the simplest and most widely used. This paper is based on the general method of the N.A.C.A. report and presents, in particular, the application of the report to elliptical and circular frames. In addition, some general simplifications based on symmetry and load conditions are presented.

No attempt has been made to break down the analysis into a number of specific solutions, but rather simplifications of the basic equations are presented which apply to any loading condition.

A set of curves is presented at the end of this article from which the length, moment of length, and moment of inertia of the length of an ellipse may be determined.

INTRODUCTION

THE GENERAL EQUATIONS of reference 1 are modified in this paper to facilitate their application to symmetric rings and rings of circular or elliptical shape. The modifications and simplifications are listed below. Steps I, II, III, and IV deal with specific properties of the sections and are progressive in that Step II embodies Step I, and Step III embodies Steps I and II. Steps V through VII depend on the type of loading.

Step I—Simplifications Due to Symmetry.
Step II—Cancellation of *EI* Terms (Homogeneous Material—Constant Cross Section).
Step III—Simplifications Due to Elliptical Shape.
Step IV—Modifications Due to Splitting of Ring.
Step V—General Loading (Unsymmetric).
Step VI—Equal, Symmetrically Placed Loads.
Step VII—Equal, Asymmetrically Placed Loads.

Terminology

X_m = bending moment at cut
X_p = axial load at cut
X_v = shear at cut
M_0 = bending moment at any point in the determinate structure
M_m = bending moment at any point due to a unit bending moment at the cut
M_p = bending moment at any point due to a unit axial load at the cut

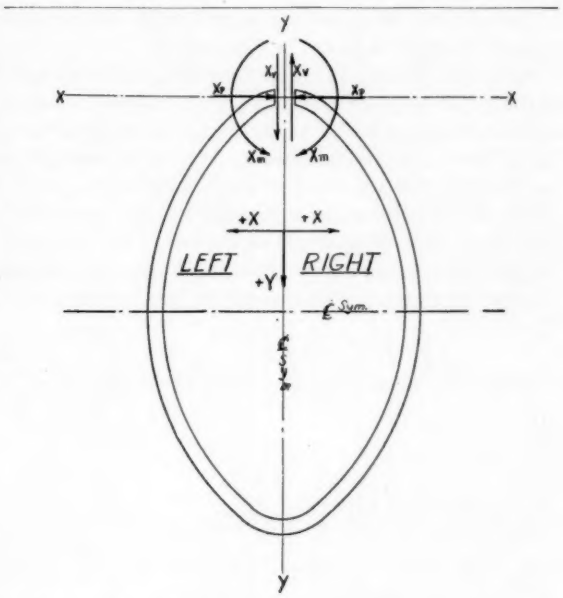

FIG. 1. This figure illustrates the sign conventions used throughout this paper.

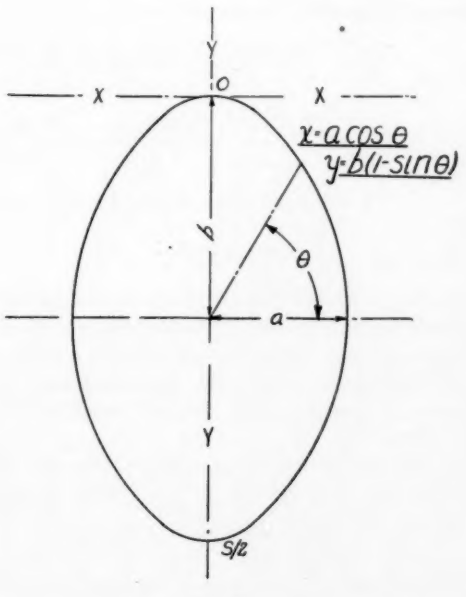

FIG. 2.

Received April 21, 1942.

* The opinions expressed in this article are those of the author and are not necessarily endorsed by the C.A.A.

† Associate Aeronautical Engineer.

M_v = bending moment at any point due to a unit shear load at the cut

ds = element of length

Subscripts L and R refer to left- and right-hand sides of the ring, respectively.

$$M_L = M_{0L} + M_{mL}X_m + M_{pL}X_p + M_{vL}X_v$$

$$M_R = M_{0R} + M_{mR}X_m + M_{pR}X_p + M_{vR}X_v$$

where, by definition:

$$\left.\begin{aligned} M_{mL} &= M_{mR} = 1 \\ M_{pL} &= M_{pR} = y \\ M_{vL} &= x \\ M_{vR} &= -x \end{aligned}\right\} \quad \text{see Fig. 1}$$

Step I

The unknown loads at an assumed cut in the top of a symmetric ring are given below. The derivation of these expressions may be found in reference 1.

Although the origin or point of action of these loads could have been assumed to be at any point in the plane of the bulkhead, past experience with bulkhead analysis has shown that from the point of view of work involved, in order to arrive finally at the stresses at any particular section of the bulkhead, the most logical origin is at the top or bottom of the bulkhead. It is to be remembered that the main part of the work in bulkhead analysis is not the determination of the unknown forces required to make the structure determinate but the determination of the effects of these redundant loads on the structure in connection with the known external loads and reactions. The assumption of an origin at the top of the ring leads to a simple convention of signs (as shown in Fig. 1). In addition, if the loading is complicated and a graphic method is resorted to for the determination of M_0, V_0, and P_0, the calculations are simplified by the fact that each half of the frame can be treated as a separate cantilever.

$$X_m = \frac{\left(2\int\frac{y\,ds}{EI}\right)\left[\int\left(\frac{M_0 y}{EI}\right)_L ds + \int\left(\frac{M_0 y}{EI}\right)_R ds\right] - \left(2\int\frac{y^2}{EI}\,ds\right)\left[\int\left(\frac{M_0}{EI}\right)_L ds + \int\left(\frac{M_0}{EI}\right)_R ds\right]}{\left(2\int\frac{ds}{EI}\right)\left(2\int\frac{y^2\,ds}{EI}\right) - \left(2\int\frac{y\,ds}{EI}\right)^2} \tag{1}$$

$$X_p = \frac{\left(2\int\frac{y\,ds}{EI}\right)\left[\int\left(\frac{M_0}{EI}\right)_L ds + \int\left(\frac{M_0}{EI}\right)_R ds\right] - \left(2\int\frac{ds}{EI}\right)\left[\int\left(\frac{M_0 y}{EI}\right)_L ds + \int\left(\frac{M_0 y}{EI}\right)_R ds\right]}{\left(2\int\frac{ds}{EI}\right)\left(2\int\frac{y^2\,ds}{EI}\right) - \left(2\int\frac{y\,ds}{EI}\right)^2} \tag{2}$$

$$X_v = -\left[\int (M_0 x/EI)_L\,ds - \int (M_0 x/EI)_R\,ds\right]/(2\int x^2\,ds/EI) \tag{3}$$

Step II

If the ring is made of homogeneous material and is of constant cross section (or nearly so), the "EI" terms cancel out and the above equations become:

$$X_m = \frac{(2\int y\,ds)[\int (M_0 y)_L\,ds + \int (M_0 y)_R\,ds] - (2\int y^2\,ds)[\int (M_0)_L\,ds + \int (M_0)_R\,ds]}{4(\int ds)(\int y^2\,ds) - (2\int y\,ds)^2} \tag{1a}$$

$$X_p = \frac{(2\int y\,ds)[\int (M_0)_L\,ds + \int (M_0)_R\,ds] - (2\int ds)\,[\int (M_0 y)_L\,ds + \int (M_0 y)_R\,ds]}{4(\int ds)(\int y^2 ds) - (2\int y\,ds)^2} \tag{2a}$$

$$X_v = -[\int (M_0 x)_L\,ds - \int (M_0 x)_R\,ds]/2\int x^2\,ds \tag{3a}$$

Step III

Eqs. (1a), (2a), and (3a) are the general equations for a symmetric ring of any geometric shape. Since this paper is concerned primarily with rings of elliptical or circular section, the integrals depending only on the geometric properties of the ring are completely determined below.

The five basic integrals to evaluate are: (a) $\int_0^{s/2} ds$, (b) $\int_0^{s/2} y\,ds$, (c)* $\int_0^{s/2} x\,ds$, (d) $\int_0^{s/2} y^2\,ds$, and (e) $\int_0^{s/2} x^2\,ds$.

* Due to symmetry, this integral does not appear, but its evaluation proves useful for the solution of other problems.

Evaluation of Integrals

Let

Q_1 = complete elliptic integral of the first kind

$= \int_0^{\pi/2} d\theta/\sqrt{1 - k^2\sin^2\theta}$

Q_2 = complete elliptic integral of the second kind

$= \int_0^{\pi/2}\sqrt{1 - k^2\sin^2\theta}\,d\theta$

$k^2 = (b^2 - a^2)/b^2$

where a and b are the semimajor and semiminor axes of the ellipse, respectively, and θ is the basic parameter as shown in Fig. 2

(a) $\int_0^{s/2} ds = 2bQ_2$ (b) $\int_0^{s/2} y\,ds = 2b^2Q_2$

(c) $\int_0^{s/2} x\,ds = ab/k(\sin^{-1} k + k\sqrt{1-k^2})$

(d) $$\int_0^{s/2} y^2\,ds = 2b^3Q_2 + 2b^3\left[\left(\frac{2k^2-1}{3k^2}\right)Q_2 + \left(\frac{1-k^2}{3k^2}\right)Q_1\right]$$

(e) $$\int_0^{s/2} x^2\,ds = 2a^2bQ_2 - 2a^2b\left[\left(\frac{2k^2-1}{3k^2}\right)Q_2 + \left(\frac{1-k^2}{3k^2}\right)Q_1\right]$$

Numerical values of these integrals are determined from graphs or tables at the end of this paper. It should be noted that the denominators and part of the numerators of Eqs. (1a), (2a), and (3a) are now completely determined.

STEP IV

(a) In many practical aircraft structures, it is necessary to make a cut in the ring. It is customary, when this is done, to run stringers from the cut to the adjacent bulkheads.

In the event that there are no stringers, the problem is no longer statically indeterminate because X_m, X_p, and X_v may be assumed to be zero at the free ends.

Assuming now that stringers are present, let F = resisting force offered by the stringer. It is assumed that the stringer has no torsional stiffness and that the stringer stiffness is negligible compared to the skin stiffness.

It follows that under these circumstances X_m and X_p will be zero at the cutout and that the stiffener deflection perpendicular to the plane of the skin at the cutout is the only deflection that need be considered in the equations of internal strain energy.

Determination of Internal Energy of Stiffener

The stringer is considered as a fixed-ended beam. Let:

L = length of stiffener joining bulkheads adjacent to split ring
c = distance from one bulkhead to split ring
$d = L - c$

Then the deflection $\delta = (1/3)(Fc^3d^3/EI_sL^3)$.

U = internal energy of stiffener = $(1/6)F^2c^3d^3/EI_sL^3$

$$dU/dF = (1/3)Fc^3d^3/EI_sL^3$$

It should be noted that $F = X_v$, since it has been assumed that this is the only force acting at the cut.

$$\frac{\partial u}{\partial X_v} = \int \frac{M}{EI}\,M_v\,ds + \frac{X_vc^3d^3}{3EI_sL^3} = 0$$

Since the ring is symmetric,

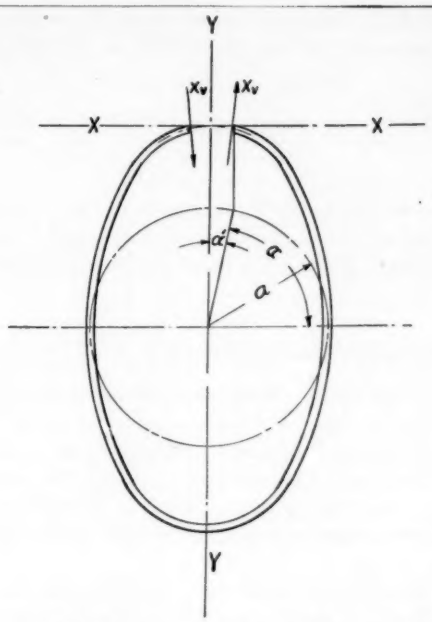

FIG. 3. This figure shows the line of action of X_v for a split ring with stiffeners.

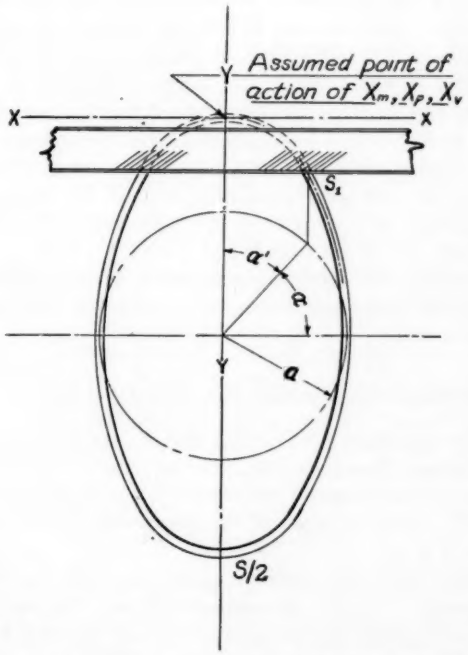

FIG. 4. Location of axes for split ring with fixed ends.

$$\frac{\partial u}{\partial X_v} = 0 = \int (M_0x)_L\,ds - \int (M_0x)_R\,ds + 2X_v\int x^2\,ds + \left(\frac{X_vc^3d^3I}{3L^3I_s}\right)_L + \left(\frac{X_vc^3d^3I}{3L^3I_s}\right)_R = 0$$

where I_s = moment of inertia of the stringer and I = moment of inertia of section through side of ring.

$$X_v = -\frac{\int (M_0 x)_L \, ds - \int (M_0 x)_R \, ds}{2\int x^2 \, ds + (2/3)c^3 d^3 I/L^3 I_s}$$

The above equation assumes that the loads are distributed in such a manner as to cause equal X_v loads on either side. If the cut is small, this will normally be the case.

Split Ring with Ends Rigidly Fixed

(b) Bulkheads at wing spars are often discontinuous through the spar and rigidly attached to it. If the spar is assumed infinitely stiff compared to the bulkhead ring, no deflection can occur in the spar itself and no work can be done. If this is the case, the bulkhead becomes a split ring with unknown loads at the ends.

A solution may be accomplished by making a hypothetic cut through the spar and integrating only over the periphery of the ring (see Fig. 4). It is necessary to integrate only over the ring itself, since it has been assumed that the spar is infinitely stiff compared with the ring. This fact may readily be detected from Eqs. (1), (2), and (3) where the stiffness is represented by the factor EI, which in all the integrals appears in the denominator. It is obvious that if the EI term over part of the path of integration is large compared to its magnitude over the rest of the path, then the contribution of the first part to the total value of the integral is small, and no serious error is introduced by omitting the first part of the integration.

Keeping the above facts in mind, it is possible to write the basic equations for a split ring with fixed ends.

Basic Equations for a Split Ring with Fixed Ends

The equations for X_m, X_p, and X_v are symbolically the same as Eqs. (1a), (2a), and (3a), the only difference being in the limits of integration. The limits are now s and $s/2$, or in terms of the parameter θ, $\theta = \alpha'$ to $\theta = -\pi/2$.

This change of limits requires that the five basic integrals of Step III be evaluated again. The terminology is the same as that of Step III with the addition of the following expressions:

$$K_1 = \int_0^\alpha d\theta / \sqrt{1 - k^2 \sin^2 \theta}$$

$$K_2 = \int_0^\alpha \sqrt{1 - k^2 \sin^2 \theta}\, d\theta$$

(f) $$\int_{s_1}^{s/2} ds = b(Q_2 + K_2)$$

(g) $$\int_{s_1}^{s/2} y\, ds = b^2(Q_2 + K_2) + \frac{b^2 k \cos\alpha}{2}\sqrt{\frac{1-k^2}{k^2} + \cos^2\alpha} + \left(\frac{1-k^2}{2k}\right)b^2 \times \left[\log_e\left(\cos\alpha + \sqrt{\frac{1-k^2}{k^2} + \cos^2\alpha}\right) - \log_e\sqrt{\frac{1-k^2}{k^2}}\right]$$

(h) $$\int_{s_1}^{s/2} x\, ds = \frac{kab}{2}\left\{\sin\alpha\sqrt{\frac{1}{k^2} - \sin^2\alpha} + \frac{1}{k^2}\sin^{-1} k\sin\alpha + \sqrt{\frac{1}{k^2} - 1} - \frac{1}{k^2}\sin^{-1}(-k)\right\}$$

(i) $$\int_{s_1}^{s/2} y^2\, ds = b^3(Q_2 + K_2) + b^3 k\cos\alpha\sqrt{\frac{1-k^2}{k^2} + \cos^2\alpha} + \left(\frac{1-k^2}{k}\right)b^3\left[\log_e\left(\cos\alpha + \sqrt{\frac{1-k^2}{k^2} + \cos^2\alpha}\right) - \log_e\sqrt{\frac{1-k^2}{k^2}}\right] - \frac{b^3}{3}\sqrt{\sin^2\alpha - (1+k^2)\sin^4\alpha + k^2\sin^6\alpha} + b^3\left[\left(\frac{2k^2-1}{3k^2}\right)(Q_2 + K_2) + \left(\frac{1-k^2}{3k^2}\right)(Q_1 + K_1)\right]$$

(j) $$\int_{s_1}^{s/2} x^2\, ds = a^2 b(Q_2 + K_2) + \frac{a^2 b}{3}\sqrt{\sin^2\alpha - (1+k^2)\sin^4\alpha - k^2\sin^6\alpha} - a^2 b\left[\left(\frac{2k^2-1}{3k^2}\right)(Q_2 + K_2) + \left(\frac{1-k^2}{3k^2}\right)(Q_1 + K_1)\right]$$

These equations are solved for various values of α, and the results plotted at the end of this paper. In applying these results, it is to be remembered that the origin was chosen at the top of the ellipse. Although, because the ring is split, the origin is now only a point in space, this does not preclude its being the point of action of the unknown loads. It is to be remembered that any point in space could have been chosen as the origin, provided that the values of the integrals were calculated with reference to that point. Eqs. (f) through (j) are derived on the basis of the origin's being at the top of the hypothetic ellipse. Therefore the substitution of values from these equations ((f) through (j)) in Eqs. (1a), (2a), and (3a) yields a set of redundants which act at the top of the hypothetic ellipse. This fact should be kept in mind when determining the effects of X_m, X_p, and X_v on the determinate loads on the frame.

STEP V

In many cases, complicated loadings may be broken down into the simple loadings of Steps VI and VII,

and the principle of superposition applied. When this is not possible, the general equations of Steps II and IV must be applied directly.

Step VI

When the loads on both sides are equal and symmetrically placed, the integrals containing M_0 have the same numerical value on either side of the cut and the left-and right-hand summations may be combined. It should be noted that under these conditions the integrals $\int M_0\,ds$ and $\int M_0 y\,ds$ need only be calculated for one-half of the ring and that the integral $\int M_0 x\,ds$ disappears from the equations.

The equations of Steps II and IVb become:

$$X_m = \frac{(4\int y\,ds)(\int M_0 y\,ds) - (4\int y^2\,ds)(\int M_0\,ds)}{D} \tag{1b}$$

$$X_p = \frac{(4\int y\,ds)(\int M_0\,ds) - (4\int ds)(\int M_0 y\,ds)}{D} \tag{2b}$$

$$X_v = 0 \tag{3b}$$

where $D = 4(\int ds)(\int y^2\,ds) - (2\int y\,ds)^2$

The equation of Step IVa becomes $X_v = 0$.

No attempt has been made to evaluate the integrals $\int M_0\,ds\ \int M_0 y\,ds$ for any specific loading condition because there are any number of load distributions that may be classified as "symmetric loadings," and, as stated in the abstract, it is not the purpose of this paper to give a number of specific solutions.

If the loading is such that the integrals containing M_0 do not lend themselves to simple analytical solution, standard numerical or graphic methods should be used.

Step VII

When the loads on both sides are symmetrically placed but at in opposite directions, it is possible (as in Step VI) to combine the left- and right-hand summations. In this case it should be noted that the integrals $\int M_0\,ds$ and $\int M_0 y\,ds$ disappear and that the integral $\int M_0 x\,ds$ need only be calculated for one side.

The equations of Steps II and IVb become

$$X_m = 0 \tag{1c}$$

$$X_p = 0 \tag{2c}$$

$$X_v = -\frac{2\int M_0 x\,ds}{2\int x^2\,ds} = -\frac{\int M_0 x\,ds}{\int x^2\,ds} \tag{3c}$$

The equation of Step IVa becomes

$$X_v = -\frac{2\int M_0 x\,ds}{2\int x^2\,ds + (2/3)c^3d^3I/L^3I_s} = -\frac{\int M_0 x\,ds}{\int x^2\,ds + (1/3)c^3d^3I/L^3I_s}$$

Table 1

Evaluation of $\int_{s_1}^{s/2} ds/b$

α'	$k = 0$	0.1737	0.500	0.707	0.866
0	3.1416	3.1178	2.9350	2.7012	2.4222
10	2.9671	2.9459	2.7836	2.5772	2.3336
20	2.7925	2.7738	2.6307	2.4496	2.2377
30	2.6180	2.6015	2.4751	2.3156	2.1295
40	2.4435	2.4287	2.3158	2.1732	2.0065
50	2.2689	2.2555	2.1526	2.0221	1.8686
60	2.0944	2.0818	1.9854	1.8626	1.7172
70	1.9199	1.9078	1.8148	1.6962	1.5549
80	1.7453	1.7334	1.6418	1.5247	1.3850
90	1.5708	1.5589	1.4675	1.3506	1.2111

Table 2

Evaluation of $\int_{s_1}^{s/2} y\,ds/b^2$

α'	$k = 0$	0.1737	0.500	0.707	0.866	$\alpha°$
0	3.1416	3.1178	2.9350	2.7012	2.4222	90°
10	3.1407	3.1069	2.9329	2.7008	2.4214	80°
20	3.1345	3.1044	2.9323	2.6962	2.4182	70°
30	3.1180	3.0832	2.9137	2.6831	2.4079	60°
40	3.0863	3.0572	2.8854	2.6575	2.3855	50°
50	3.0349	3.0046	2.8362	2.6122	2.3446	40°
60	2.9604	2.9346	2.7658	2.5444	2.2800	30°
70	2.8596	2.8249	2.6670	2.4489	2.1860	20°
80	2.7301	2.7072	2.5374	2.3209	2.0601	10°
90	2.5708	2.5446	2.3796	2.1656	1.9011	0°

Table 3

Evaluation of $\int_{s_1}^{s/2} x\,ds/ab$

α'	$k = 0$	0.1737	0.500	0.707	0.866	$\alpha°$
0	2.0000	1.9897	1.9132	1.8181	1.7092	90°
10	1.9848	1.9747	1.9003	1.8067	1.7011	80°
20	1.9397	1.9301	1.8608	1.7737	1.6762	70°
30	1.8660	1.8575	1.7954	1.7169	1.6303	60°
40	1.7660	1.7586	1.7037	1.6353	1.5597	50°
50	1.6428	1.6362	1.5884	1.5285	1.4622	40°
60	1.5000	1.4940	1.4516	1.3981	1.3383	30°
70	1.3420	1.3367	1.2972	1.2473	1.1913	20°
80	1.1736	1.1683	1.1301	1.0817	1.0274	10°
90	1.0000	0.9947	0.9569	0.9088	0.8544	0°

Table 4

Evaluation of $\int_{s_1}^{s/2} y^2\,ds/b^3$

α'	$k = 0$	0.1737	0.500	0.707	0.866	$\alpha°$
0	4.7124	4.6672	4.3498	3.9375	3.4396	90°
10	4.7124	4.6487	4.3473	3.9375	3.4389	80°
20	4.7121	4.6570	4.3566	3.9374	3.4494	70°
30	4.7105	4.6448	4.3475	3.9352	3.4383	60°
40	4.7047	4.6506	4.3433	3.9313	3.4344	50°
50	4.6892	4.6314	4.3267	3.9162	3.4217	40°
60	4.6571	4.6082	4.2981	3.8879	3.3943	30°
70	4.5986	4.5691	4.2404	3.8333	3.3393	20°
80	4.5021	4.4589	4.1423	3.7369	3.2458	10°
90	4.3562	4.3058	3.9992	3.5986	3.0998	0°

TABLE 5

Evaluation of $\int_{s_1}^{s/2} X^2\, ds/a^2b$

α'	$k = 0$	0.1737	0.500	0.707	0.866	$\alpha°$
0	1.5708	1.5684	1.5202	1.4651	1.4048	90°
10	1.5691	1.5651	1.5185	1.4639	1.4039	80°
20	1.5570	1.5524	1.5080	1.4550	1.3970	70°
30	1.5255	1.5216	1.4799	1.4310	1.3775	60°
40	1.4680	1.4638	1.4275	1.3837	1.3366	50°
50	1.3807	1.3778	1.3457	1.3082	1.2675	40°
60	1.2637	1.2610	1.2335	1.2009	1.1657	30°
70	1.1207	1.1186	1.0936	1.0645	1.0227	20°
80	0.9582	0.9555	0.9325	0.9049	0.8744	10°
90	0.7854	0.7834	0.7600	0.7326	0.7024	0°

Evaluation of Integrals for Values of k and α'

Curves are plotted for $\alpha = 0°, 10°, 20°, 30°, 40°, 50°, 60°, 70°, 80°, 90°$.

The value of the integral in question is taken as the ordinate and $\beta = \sin^{-1} k$ is taken as the abscissa. It should be noted at this point that $\beta = 0$ represents a circle.

The integrals were evaluated for the five values of β given below.

k^2	k	β
0.000	0.0000	0°
0.030	0.1737	10°
0.250	0.5000	30°
0.500	0.7070	45°
0.750	0.8660	60°

The results of the evaluations in Tables 1–5 are given in a dimensionless form and may be applied to an ellipse of any size.

Use of Curves

The curves given in Figs. 5, 6, 7, 8, and 9 are general and represent (1) the length of an elliptical arc, (2) the moment of length about the X axis, (3) the moment of length about the Y axis, (4) the moment of inertia of the length about the X axis, and (5) the moment of inertia of the length about the Y axis.

The denominators of the expressions for X_m, X_p, and X_v are completely determined from these curves, but only part of the numerators can be found from them.

It may be possible (depending on the type of loading) to evaluate the terms containing M_0 in a manner similar to that used for the terms depending only on the shape, but it is advisable when the loading is complicated to determine the values graphically.

These curves may also be used for rings of oval shape when there is not too much deviation from an elliptical shape.

Range of Curves

a/b varies from 1 to $1/2$ and α varies from 0° to 90°.

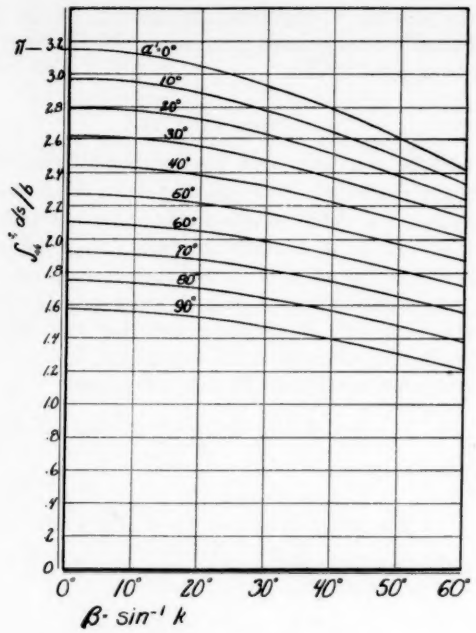

FIG. 5. $\int ds/b$ vs. $\beta = \sin^{-1} k$.

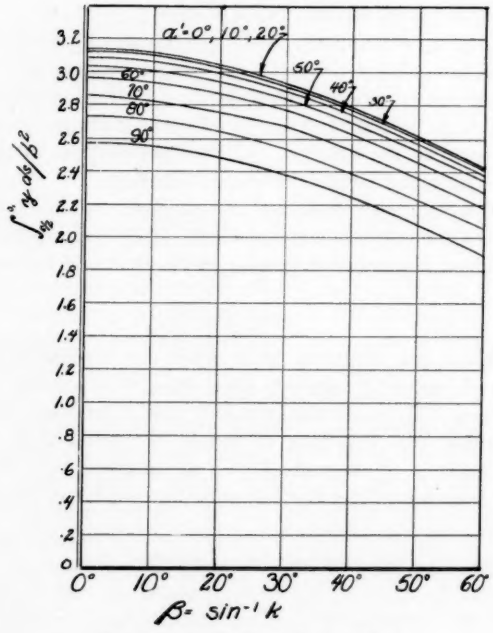

FIG. 6. $\int y\, ds/b^2$ vs. $\beta = \sin^{-1} k$.

Application of Formulas to Fuselage Rings

Before it is possible to determine the loads in the determinate structure, it is necessary to put the bulkhead in balance by skin reactions. This may easily be done by using the basic concepts of shear flow, keeping in mind that the shear distribution over a section in the region of a concentrated load does not exactly follow the law that:[2]

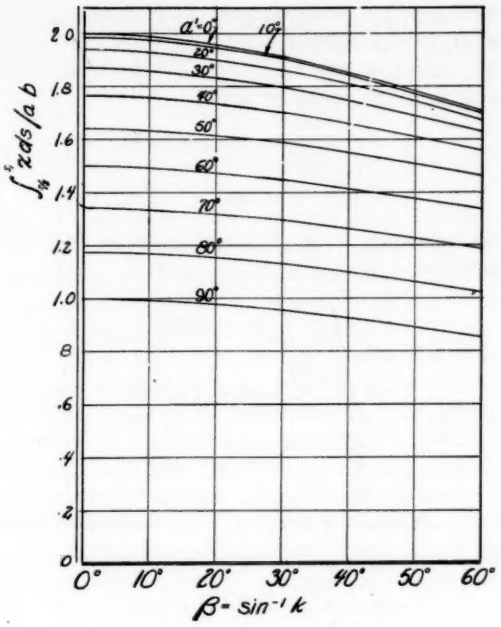

FIG. 7. $\int x\,ds/ab$ vs. $\beta = \sin^{-1} k$.

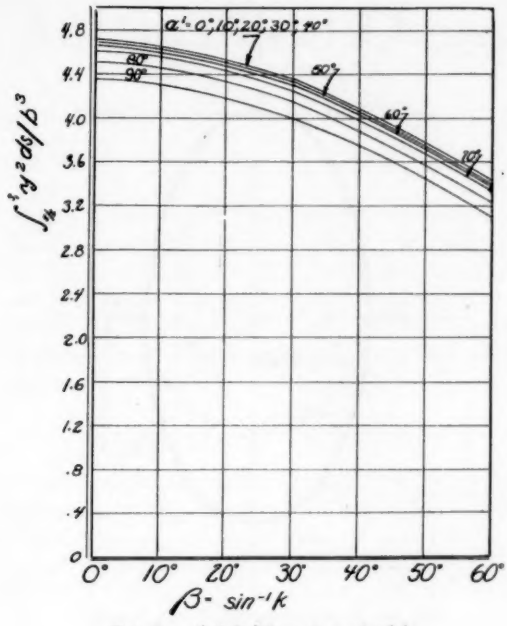

FIG. 8. $\int y^2\,ds/b^3$ vs. $\beta = \sin^{-1} k$.

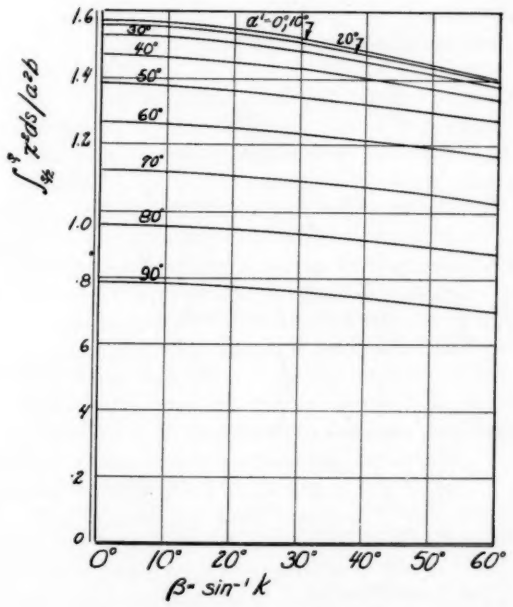

FIG. 9. $\int x^2\,ds/a^2b$ vs. $\beta = \sin^{-1} k$.

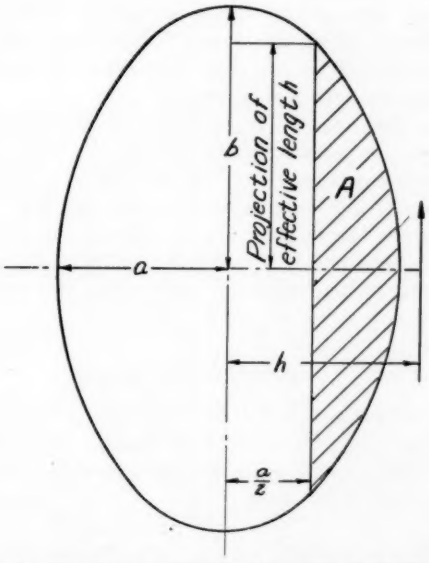

FIG. 10. The shear center for the assumed distribution is given by the formula $h = a/2 + 2A/y$, where h = distance from Y axis to shear center, A = shaded area, and y = projection of effective length on the Y axis.

$$q = VQ/I$$

where:

q = shear in pounds per inch
V = vertical shear in pounds
I = moment of inertia of section
Q = static moment of area

The shear distribution determined by the above formula would give a maximum running shear in the skin at the neutral axis of the skin cross section. Actually, the running shear loads are nearly constant over the entire periphery, and it is sufficiently accurate for purposes of bulkhead analysis to assume constant running load over an effective length of skin. The effective length of skin may be assumed to be that length of skin outside a line drawn parallel to the Y axis through $x = a/2$ (see Fig. 10). The projected shear per inch is determined by dividing the load required

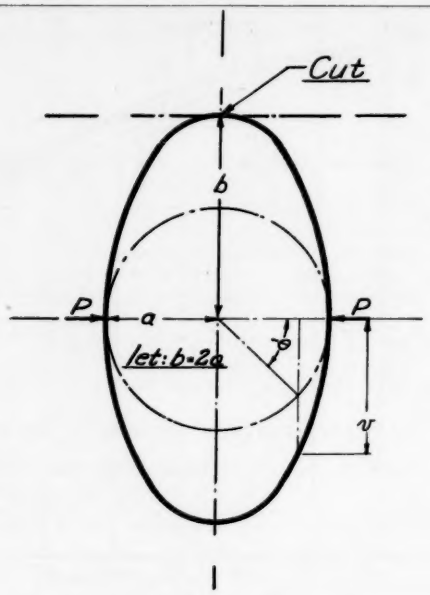

FIG. 11. Loading for illustrative example.

for balancing (applied at the shear center of the effective skin segment) by the projection of the length of the segment along the Y axis. The actual shear per inch in the skin at any point is equal to the projected shear per inch as defined above.

Once the ring has been balanced, the determinate moments, shears, and axial loads (M_0, V_0, and P_0) may be determined at any point by treating each half of the ring as a cantilever with its free end at the cut.

All the integrals may now be evaluated and X_m, X_p, and X_v determined. The total loads at any point are found to be the algebraic addition of the effects of X_m, X_p, and X_v to M_0, V_0, and P_0.

ILLUSTRATIVE EXAMPLE

The problem shown in Fig. 11 is now solved to illustrate the use of the tables and curves. Since the ring and loading are symmetric, the equations developed under Step VI are used.

The integrals to evaluate are: $\int ds$, $\int y\,ds$, $\int y^2\,ds$, $\int M_0\,ds$, and $\int M_0 y\,ds$.

The values of the first three integrals are found directly from the curves or tables.

$$k^2 = [(2a)^2 - a^2]/(2a)^2 = 0.75$$
$$k = 0.866$$
$$\beta = \sin^{-1} k = 60^\circ$$

The following values of the integrals are determined from Tables 1, 2, and 4.

$$\int_{+\pi/2}^{-\pi/2} ds = 2.4222b$$
$$\int_{+\pi/2}^{-\pi/2} y\,ds = 2.4222b^2$$
$$\int_{+\pi/2}^{-\pi/2} y^2\,ds = 3.4396b^3$$

The integrals containing M_0 are evaluated as follows:

$$M_0 = Pv = Pb\sin\theta$$
$$ds = b\sqrt{1 - k^2\sin^2\theta}\,d\theta$$
$$\int_0^{-\pi/2} M_0\,ds = Pb^2\int_0^{-\pi/2} \sin\theta\sqrt{1 - k^2\sin^2\theta}\,d\theta$$

Performing the above integration,

$$\int_0^{-\pi/2} M_0\,ds = Pb^2(0.69006)$$
$$y = b(1 - \sin\theta)$$
$$\int_0^{-\pi/2} M_0 y\,ds = Pb^3\int_0^{-\pi/2} \sin\theta(1 - \sin\theta)\times\sqrt{1 - k^2\sin^2\theta}\,d\theta$$
$$= Pb^3\int_0^{-\pi/2} \sin\theta\sqrt{1 - k^2\sin^2\theta}\,d\theta - \int_0^{-\pi/2} \sin^2\theta\sqrt{1 - k^2\sin^2\theta}\,d\theta$$

Performing the above integration,

$$\int_0^{-\pi/2} M_0 y\,ds = 1.19880Pb^3$$

Substituting the above results in Eqs. (1b), (2b), and (3b),

$$X_m = \frac{4(2.4222b^2)(1.19880Pb^3) - 4(3.4396b^3)(0.69006Pb^2)}{4(2.4222b)(3.4396b^3) - [2(2.4222b^2)]^2} = 0.21515Pb$$

$$X_p = \frac{4(2.4222b^2)(0.69006Pb^2) - 4(2.4222b)(1.19880)Pb^3}{4(2.4222b)(3.4396b^3) - [2(2.4222b^2)]^2} = 0.50004P$$

$$X_p = 0$$

It should be noted that X_p could have been determined by inspection as equal to $P/2$, due to the fact that the loading is symmetric about two axes.

REFERENCES

[1] Lundquist, E. E., and Burke, W. F., *General Equations for the Stress Analysis of Rings*, N.A.C.A. T.R. No. 509, 1934.

[2] Timoshenko, S., *Theory of Elasticity*, pp. 48, 49; McGraw-Hill Book Company, New York, 1934.

[3] von Kármán, Th., and Biot, M. A., *Mathematical Methods in Engineering*, pp. 119–129; McGraw-Hill Book Company, New York, 1940.

Vision, Hearing, and Aeronautical Design

LEON D. CARSON*, WALTER R. MILES†, AND S. S. STEVENS‡
U.S. Navy, Yale University School of Medicine, and Harvard University

IT IS PRINCIPALLY through the sense of vision that pilots are aware of the nature of terrain, weather conditions, the terrestrial orientation of their aircraft, and the position and movements of enemy planes. Even so-called "blind flying" is primarily a visual function. Here the "contact" is transferred from the horizon and ground objects to the special instruments upon the panel. Hearing likewise is of critical importance to military flyers in that command information and assistance from ground control stations must be audible over the communication system. Also, intercommunication systems within aircraft must function as the principal means of maintaining prompt and coordinated action of members of air crews in carrying out military missions effectively. These facts are generally known and accepted by plane designers. However, engineering success in providing for ease of seeing and ease of hearing is quite variable, and these basic pilot requirements merit continued attention.

Take, for example, the almost complete blanking off from vision of an area directly ahead of the pilot when a plane changes its normal flight attitude to a landing attitude. This is particularly vicious in the case of fighter aircraft with large air-cooled engines in the nose of the ship, and the condition has resulted in a great number of avoidable landing, taxiing, and take-off accidents. Aircraft carrier accidents have undoubtedly resulted from this blanked-off area, in spite of the fact that a landing signal officer is supposed to direct the landing properly. Mirror reflections of the area immediately ahead of the plane could be provided. Tricycle landing gear on some few aircraft have done much to benefit this blindness due to radical change in plane attitude.

Engineers are no doubt aware of the desirability of placing pilots, observers, and gunners as near as possible to the transparent panels through which they must get their visual impressions. The nearer the eye is to the window, the larger the visual field that can be seen through it or, for a given angular field, the smaller the window needed. The ordinary spectacle lens $1\frac{1}{2}$ in. in diameter gives the wearer an uninterrupted view of almost 90°. Proximity to airplane windows also makes for clear visual fields: (1) It is easier to provide the requisite transparent area free from obstructing pillars, panel joints, and opaque accessories; (2) marks, specks, and scratches on the window surfaces are less bothersome because they are out of focus; and (3) when near the window, the observer's head makes an area of shadow which is helpful, particularly at night, since it blocks off reflections from the inner surface.

Presented at the Physiologic Problems Session, Eleventh Annual Meeting, I.Ae.S., New York, January 25–29, 1943.

* Medical Research Section, Bureau of Aeronautics.
† Professor of Psychology.
‡ Director, Psycho-Acoustic Laboratory.

THE GUNNER'S VISUAL PROBLEM

The position of gunners in relation to windows is especially worthy of consideration. Take a hypothetic set of measurements for discussion. The gunner's eye must be about 9 in. behind the gunsight; the sight is 20 in. from the aiming panel; the gunner's seat is therefore placed against the back wall of the turret, and the space in front of him is well filled with gun supporting and operating structures. The aiming panel is a beautifully clear, optically perfect surface 14 by 14 in. The engineers are to be congratulated on this window but not on the position of the gunner. For him the situation resembles that met in tunnel vision. His eyes are 29 in. away from this superb window which can provide him with a view of only 28°—that is, 28° of the full 60° to 90° that are so critically needed.

The aiming panel must, of course, be well mounted, and this calls for a rather heavy metal frame. Sometimes it is as much as 2 in. wide. Other small, usually curved windows border the aiming panel, and each of these must have or share a frame with adjoining windows or wall structures. When the guns are in front of the gunner, sections of the mounting structure, brackets, electrical switches, etc., frequently have locations that obscure portions of the windows from the gunner's eyes. The total effect is a lattice window with the lattice predominating over the clear space in some instances. From the gunner's view through a particular panel, a total of only 25 per cent is unobstructed to binocular vision; 53 per cent is totally obstructed; 22 per cent is obstructed for one eye. For the gunner the irregular lattice is a hazard to vision and life. It is true enough that through the lattice he can see a lot of landscape as he looks from one opening to another. What he needs to see, however, is moving planes. When his eyes catch sight of one, they try to follow it. This is done by a special kind of coordination in the action of eye muscles and is known as pursuit eye movement. The eye actively glides along at a rate set by the visual target and appropriate to keep it in clearest possible view on the fovea. Visibil-

ity of the moving target is essential for this type of seeing. Whenever the moving target momentarily disappears, as happens when it passes behind opaque lattice areas, the pursuit movement is immediately stopped. The eye jumps to the far edge of the obstruction and waits. When the target emerges, a new pursuit movement must be organized by the nervous system. This necessarily costs an average delay of 0.15 of a precious second before clear pursuit vision can be re-established. The gunner is, of course, not completely blind during this interval, but his visual efficiency on the moving target is hampered by every opaque gap across which he is compelled to operate.

In turrets where the guns may be mounted at the sides and rather low down, it should be possible to reduce the amount of structure in front of the gunner and to bring him forward much nearer the front panel. This will increase his angle of uninterrupted view, make visual pursuit of his targets easier, and reduce the blinding effect from the flashes of his own guns.

Vision Inside the Cockpit

Inside the cockpit there is a confusing multiplicity of instruments, and a lack of a suitable grouping of essential flying instruments according to a well-planned pattern for visual perception is noticed. For purposes of night flying, where visual function is largely dependent upon maintenance of dark adaptation of the eye, instrument panels in general are subject to the following serious faults:

1. There is too large an illuminated area. Instruments that are referred to infrequently are constantly illuminated.
2. The color of the transmitter or reflected light from these instruments is usually not of the spectral band least disturbing to night vision.
3. Intensity, as well as total area of illumination, is considerably too high. This is usually a criticism equally applicable to direct or indirect lighting, radioluminous, or fluorescent marked instruments. The only light that can be controlled easily both as to spectral character and brightness level is indirect red light. The use of a spectral red whose transmission band lies in the region of 600 millimicrons is recommended for instrument lighting.. The intensity of such light may be permitted to vary considerably without adverse effect upon night vision.

Transparent cockpit enclosures, although of fairly clear optical plastic, discolor with explosure to sunlight; some of them become finely checked because of temperature changes and vibration. Nearly all of them are capable of being scratched too easily, and the result is interference with vision. Measurements of visibility through plastic windows, compared with bulletproof glass and with open cockpit view, show that the glass produces a slight loss and that the loss from the plastic may be 5 or 6 times as much. Flat panes consistently provide better visibility than do curved plastic surfaces, but they may also give an increased drag. A compromise must be made between visibility and aerodynamic considerations. Rapid strides in development of better plastics are being made, and it should be possible soon to mold transparent cockpit enclosures of better grades of optical plastics in one piece. Surface hardening of such molded parts is desirable. Close attention should be given to reducing inside reflections that are particularly troublesome from concave surfaces.

In military aircraft it is often found that vision forward and to either side is fairly well provided for but that, even though the pilot may have the usual well-developed "rubber neck," he is handicapped by certain design features of his plane in seeing what may be above or aft. It is often forgotten that in actual combat pilots refuse to leave the "greenhouse" closed and must therefore use goggles. Any fixed aperture made available for the pilot's face should not be too small to permit use by a bespectacled or goggled aviator.

Airsickness and Vision

Airsickness of passengers and crew may result from unavoidable motion stimulation of the vestibular mechanism of the ear; from rapidly changing gravitational forces acting on viscera, muscles, and joints; and from apprehension and past unhappy memories of plane travel. All of these upsetting stimuli are, as a rule, less disturbing if those affected can see out and establish visual contact with the horizon, with cloud formations, and with the ground scene below. The old instructions to novices in flying should be remembered: "Never look at the up wing; watch the down wing." Many troop-carrying glider craft afford virtually no opportunity to look out and establish visual contact beyond the plane. To arrive at the scene of battle with a load of thoroughly ill troops contributes nothing to fighting morale and effectiveness. A part of the answer to this difficulty is—don't require passengers and crew to fly blind.

Hearing Suffers More Than Sight

The ears more than the eyes are subjected to environmental stress through flying. It seems to be true of modern aviation that every time the engineers increase the power and speed of our airplanes, the ears of the pilots take a greater beating. Although the ear is a magnificent little mechanism—the most intricate mechanical structure in the human body—it is a rather delicate device and one that seems ill designed for modern war. But the ear has gone to war along with the rest of the soldier, and the service it renders in the face of acoustic stress is to be admired.

Airplanes have always been noisy, and they are becoming noisier. A thousand horsepower fed into a propeller is able to agitate the atmosphere in a thunderous manner, and when the engine delivers 2,000 hp. the

din is doubled, or actually more than doubled, because as the tip speed of the propeller increases a larger proportion of its driving energy is converted into sound. When this energy pounds on the ear, it is striking a mechanism so sensitive that less than one quintillionth of a horsepower is needed to produce a faint sensation of hearing. In addition, more horsepower means more speed and hence, more turbulence about the ship. It is this turbulence of the slipstream over the wings and about the fuselage which produces the distressing, high-frequency random noises that sound like a mighty "shhhhhh." In some respects the noise from the turbulence about the plane is more of a problem than is the noise from the propeller itself. This is demonstrated in planes that do not have propellers. Contrary to popular notions, the interior of a glider plane moving at about 150 miles per hour is a noisy place. The noise level is about 115 db., and conversation in such a place is difficult if not impossible.

In any really fast-moving vehicle the noise is random; that is to say, all frequencies of the spectrum are present. When one listens on the ground to a plane high overhead one hears only the low frequencies of the propeller. But inside the plane it is different; there all frequencies added together at once are heard, producing a noise that is to sound what white light is to light. And as a general rule, the greater the speed, the "whiter" the noise. Also, as a general rule, the whiter the noise, the more objectionable it is to the ear. "White" noise is objectionable for three reasons: (1) It is disagreeable; (2) it produces temporary deafness; and (3) it spoils communications.

That "white" noise is annoying needs little argument. No one has been found who really enjoys it. It is true, however, that attempts to prove that long exposure to intense airplane noise is damaging to human efficiency have produced essentially negative results. When adequately motivated, a man can code a message, add columns of figures, coordinate his movements, react to a signal, etc., about as well after 8 hours in a noise of 115 db. as after a similar period in the quiet. Despite this remarkable experimental result, the subjects all report that they find the noise unpleasant, and they are happy when it is turned off.

Temporary Deafness

That airplane noise produces deafness is a well-known fact. In normal ears this deafness shows two characteristics: It is restricted more or less to the high frequencies and, fortunately, it is usually temporary. After 8 hours in an airplane noise of 115 db., the normal ear shows a hearing loss of about 40 db. in the region of 4,000 cycles. It has sometimes been supposed that low-frequency airplane noise produces high-frequency hearing loss. On the contrary, it is the high-frequency components of the noise that produce the high-frequency loss. The ear, for some unknown reason, is more vulnerable at these high frequencies.

Recovery from a 40-db. hearing loss usually occurs in about 24 hours. The recovery is rapid at first and then proceeds more slowly. About half of the loss is regained by a normal ear in the first 3 hours after exposure. Some ears apparently do not have this power of recovery, and repeated exposure to noise leaves them permanently deafened. Although the noise is usually blamed for such deafness, there is a question as to whether the ear itself is not the real culprit. At any rate, many ears appear to develop high-frequency deafness without excessive exposure to intense noise.

Improvement of Communications

The most important practical effect of airplane noise is the masking of communications. Not only is conversation impossible in some planes, but even over radio and interphone speech signals are often masked beyond recognition. Articulation tests have shown that with much of the standard military interphone equipment a listener is able to understand only about 50 per cent of the words spoken in the presence of an airplane noise of 120 db. Over the same interphones more than 95 per cent of the words are understood when there is no ambient noise present to interfere with the speech.

The difficulty of communicating under the handicap of airplane noise calls for vigorous remedies. Constructive measures can be applied in three general directions:

First, the plane can be quieted to some extent either by improved aeronautical design or by the application of sound absorbent materials. Acoustic treatment that is light enough to be tolerated in a plane does not appreciably reduce the overall noise level. It does, however, change the spectrum of the noise by reducing the intensity of the high-frequency components. Hence, the noise in an acoustically treated plane is less "white," and therefore less bothersome, than the noise in an untreated plane. Tests have shown that for the same overall sound intensity conversation person-to-person is relatively easy in a treated plane but quite impossible in an untreated one.

The second remedy calls for an improvement in the response characteristics of the communication equipment itself, especially of the microphones and earphones. A loud noise does not interfere with intelligibility nearly so much when instruments of high fidelity are used. But with microphones that have nonlinear distortion and with earphones that at some frequencies are sharply resonant, the effect of an airplane noise of 120 db. is to reduce the intelligibility of speech by 30 to 40 per cent. High-fidelity equipment is not yet being widely used in airplanes, although a few major improvements are now in process. Complete overall high fidelity from microphone to earphone must be

achieved if speech is to be transmitted to and from our most modern airplanes.

The third remedy called for by the noise problem is the shielding of the microphone and the earphones from the noise. The oxygen mask could be so designed as to shield the microphone from the ambient racket, but many otherwise excellent masks suffer from acoustic defects. This problem is now under study, and improved noise shields for hand-held microphones are being developed. The earphones and the ear of the listener can be shielded from the airplane noise by means of an acoustic socket designed to provide a tight seal against the side of the head. In present military equipment this provision has been neglected, but improved devices are now in production. Some of these ear protectors serve to reduce the unwanted sound in the aviator's ear by 20 to 50 db.

Conclusions

In general, it can be said that the problems raised by intense ambient noise are serious but not insoluble. Judicious use of sound treatment in the plane, conversion to high-fidelity microphones and earphones, and the development of acoustic devices to shield the mouth and the ears of the personnel will permit the aviator to carry on in the best noises that the aeronautical engineers are now planning to produce.

The flying and efficient fighting of modern planes are largely dependent on the special sense of vision. The eyes fortunately suffer no great decrement in function from the swift movement or high and changing elevation of the airplane. Vision is adequate to the basic task assigned to flying personnel. The chief difficulty is in providing for optimal visibility through the structures of the plane and for continuous visual check on the environment surrounding it in both day and night flying. Ideal visual conditions are not wholly attainable because of aerodynamic and structural necessities. However, the effort should be made to gain all possible visual advantages. The problem is a continuing one and offers important strategic possibilities.

Both seeing and hearing, if accompanied by prolonged attentive effort, especially under conditions of unfavorable plane design, are capable of contributing fatigue and loss of efficiency to pilot and air crew. It has been proved worth while to give the airplane engine an adequate combustive mixture by supercharging and to pay special attention to protecting the oil in the engine against "foaming" at high altitudes and reduced barometric pressures. It is proving and will prove worth while to consider the flier's eyes and ears and the rest of his mortal body and to reduce in every possible way the tendency to physiologic and psychologic "foaming" in him.

(*Continued from page 114*)

$$F = [1/(2 \sin y)][\sin (n+1)y + \sin ny - \sin y]$$

With the aid of this formula the two sums can be calculated. Substituting m for n and $2\pi/(m+1)$ for y,

$$\sum_{i=1}^{m} \cos \frac{2\pi i}{m+1} = \left[1/\left(2 \sin \frac{2\pi}{m+1}\right)\right]\left[\sin \frac{2\pi(m+1)}{m+1} + \sin \frac{2\pi m}{m+1} - \sin \frac{2\pi}{m+1}\right] = \left[1/\left(2 \sin \frac{2\pi}{m+1}\right)\right] \times \left[\sin \frac{2\pi(m+1)}{m+1} - 2 \sin \frac{2\pi}{m+1}\right] = -1$$

It can be shown in a similar way that

$$\sum_{i=1}^{m} \cos [4\pi i/(m+1)] = -1$$

Consequently,

$$N = (3/8)(m+1)$$

References

[1] Brazier, L. G., *The Flexure of Thin Cylindrical Shells and Other "Thin" Sections*, R. & M. No. 1081, 1927.

[2] Dschou, Dji-Djüän, *Die Druckfestigkeit versteifter Zylindrischer Schalen*, Luftfahrtforschung, Vol. 11, No. 8, p. 223, February, 1935.

[3] Flügge, W., *Statik und Dynamik der Schalen*, 1st Edition; Julius Springer, Berlin, 1934.

[4] Guggenheim Aeronautics Laboratory of the California Institute of Technology, *General Instability Criteria for Stiffened Metal Cylinders*, Quarterly Reports Nos. 1–5, November, 1938–July, 1940.

[5] Heck, O. S., *Ueber die Stabilität orthotroper elliptischer Zylinderschalen bei reiner Biegung*, Luftfahrtforschung, Vol. 14, No. 3, 1937.

[6] Hoff, N. J., *Instability of Monocoque Structures in Pure Bending*, Journal of the Royal Aeronautical Society, Vol. XLII, No. 328, p. 291, April, 1938.

[7] von Kármán, Th., and Tsien, Hsue-Shen, *The Buckling of Spherical Shells by External Pressure*, Journal of the Aeronautical Sciences, Vol. 7, No. 2, p. 43, December, 1939; von Kármán Th., Dunn, L. G., and Tisen, Hsue-Shen, *The Influence of Curvature on the Buckling Characteristics of Structures*, Journal of the Aeronautical Sciences, Vol. 7, No. 7, p. 276, May, 1940; von Kármán, Th., and Tsien, Hsue-Shen, *The Buckling of Thin Cylindrical Shells Under Axial Compression*, Journal of the Aeronautical Sciences, Vol. 8, No. 8, p. 303, June, 1941.

[8] Nissen, O., *Knickversuche mit versteiften Wellblechen bei reiner Druckbeanspruchung*, Jahrbuch 1937 der Deutschen Luftfahrtforschung, Vol. I, p. 452.

[9] Ryder, E. I., *General Instability of Semimonocoque Cylinders*, Air Commerce Bulletin, Vol. 9, No. 10, p. 241, April, 1938.

[10] Sechler, E. E., and Dunn, L. G., *Airplane Structural Analysis and Design*, 1st Edition; John Wiley & Sons, New York, 1942.

[11] Taylor, J. L., *Stability of a Monocoque in Compression*, R. & M. No. 1679, June, 1935.

[12] Timoshenko, S., *Theory of Elastic Stability*, 1st Edition, p. 470; McGraw-Hill Book Co., Inc., New York, 1936.

[13] Wang, Tsun-Kuei, *Buckling of Semimonocoque Structures Under Compression*, Journal of Applied Mechanics, Vol. 9, No. 3, p. A-117, September, 1942.

A Method for Rapid Estimation of Helicopter Performance

QUENTIN WALD*

United Aircraft Corporation

SUMMARY

Several papers are available which treat the analysis of rotating wing aircraft with considerable rigor and completeness. While these treatments are satisfactory for exhaustive analyses of specific helicopters, they are exceedingly complex. Since simple methods of performance estimation are available for airplanes, it is believed that a comparable system for helicopters should prove useful for comparative performance studies, preliminary estimation of characteristics of proposed designs, and determination of the effects of small changes in design. Frequently, only limited data are available for studies of this type, making elaborate analyses impossible or undesirable. The present report proposes a system of performance estimation which, it is hoped, will fulfill the need. The method is relatively simple and rapid.

The method is based on the conception of the rotor as an actuator disc and the well-known momentum relations for an actuator disc. All of the major variables in design and operation are taken into account. Comparisons have indicated that the results obtained by this system are good approximations to the results of more elaborate analysis.

In many respects this paper was suggested by Knight's paper,[3] but the method of approach is different and somewhat greater generality is obtained.

SYMBOLS USED

B = tip loss factor, assumed equal to 0.95
b = number of blades
C_T = thrust coefficient, $C_T = T/(\rho\omega^2\pi R^4/2)$
c = rotor blade chord at $r/R = 0.7$
f = equivalent parasite drag area, sq.ft.
K = ratio of effective power available at main rotor shaft to total brake power
P = engine brake power, ft.lbs. per sec.
P_i = power available to produce thrust
P_R = power required for rotor torque due to profile drag
R = rotor radius, ft.
S = resultant axial velocity ratio $(V \sin \alpha' + u)/u_0$
T = rotor normal thrust, lbs.
u = induced velocity at rotor, ft. per sec.
u_0 = induced velocity for the hovering condition
V = velocity of machine along its flight path, ft. per sec.
W = gross weight, lbs.
α = flight path angle, degrees
α' = angle between rotor tip plane and flight path
δ = rotor blade profile drag coefficient at the mean effective lift coefficient
μ = advance ratio, $= V \cos \alpha'/\omega R$
ω = rotor angular velocity, rad. per sec.
σ = rotor solidity ratio, $\sigma = bc/\pi R$
γ = angle between the rotor tip plane and a horizontal plane
ψ = blade azimuth angle (measured from down-wind position in direction of rotation)

Presented at the Rotating Wing Aircraft Session, Eleventh Annual Meeting, I.Ae.S., New York, January 25–29, 1943.

* Aeronautical Engineer, Research Division.

MOMENTUM RELATIONS

THE GENERAL MOMENTUM EQUATION for the thrust of an "actuator disc"[1, 9] is

$$T = 2\rho A u V' \tag{1}$$

where A is the effective disc area; u, the induced velocity; and V', the resultant relative wind velocity at the disc. Referring to the helicopter rotor as shown in Fig. 1

$$V'^2 = (u + V \sin \alpha')^2 + V^2 \cos^2 \alpha'$$

and $A = \pi B^2 R^2$. When $V = 0$

$$u_0^2 = T/2\rho\pi B^2 R^2 \tag{2}$$

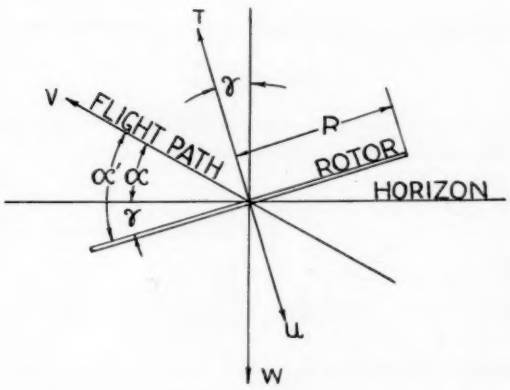

FIG. 1. Rotor geometry.

Substituting the value of T from Eq. (2) and the value of V' in Eq. (1)

$$u^4 + 2u^3 V \sin \alpha' + u^2 V^2 = u_0^4$$

eliminating $\sin \alpha'$ by the use of the following definition

$$S = (V/u_0) \sin \alpha' + (u/u_0) \tag{3}$$

and solving for V/u_0, the perfectly general momentum relation is obtained as

$$V/u_0 = \sqrt{(u_0/u)^2 + (u/u_0)^2 - 2(u/u_0)S} \tag{4}$$

This form of the momentum equation is plotted in Fig. 2, which is used in estimating performance. For reasonable values of S, when $u/u_0 < 0.20$, Eq. (4) reduces to

$$V/u_0 = u_0/u$$

In hovering flight, $T = W$. Then from Eq. (2)

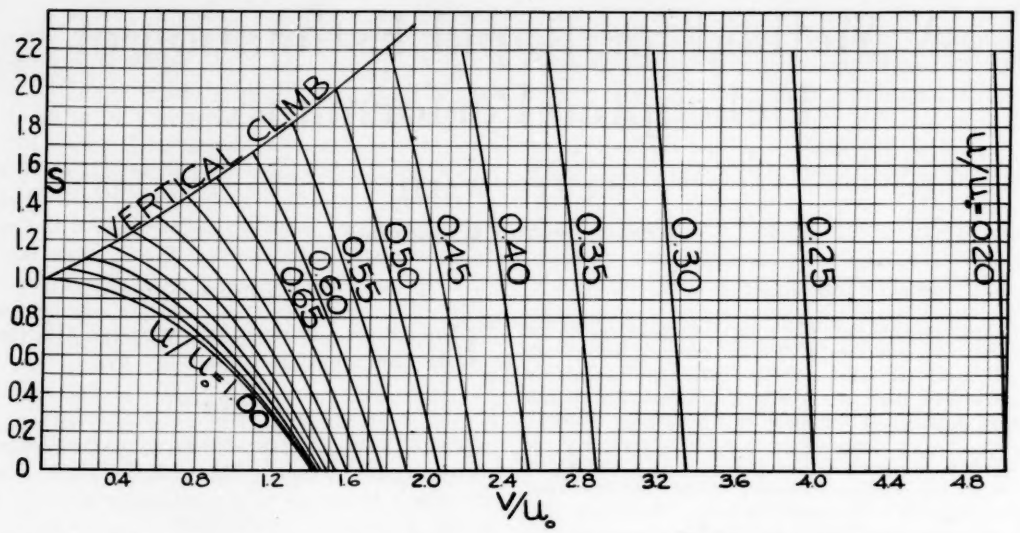

FIG. 2. Solution of the momentum equation for helicopters (Eq. 4). $V/u_0 = \sqrt{(u_0/u)^2+(u/u_0)^2-2(u/u_0)S}$, when $u/u_0 < 0.20$ $V/u_0 = u_0/u$.

$$u_0 = 15.26\left(\frac{W}{\pi R^2}\right)^{1/2}\left(\rho_0/\rho\right)^{1/2} \tag{5}$$

It will become evident that S is a useful parameter.

Rotor Speed

Since γ is always a small angle, $T = W$ is a good approximation for all flight conditions. Then

$$\frac{C_T}{\sigma} = \frac{W}{\rho\pi\omega^2R^4\sigma/2}$$

and

$$\omega = \left(\frac{2W}{\rho\pi R^4\sigma(C_T/\sigma)}\right)^{1/2} \tag{6}$$

This can be written

$$\omega = \frac{16.36}{R^2}\left(\frac{W}{\sigma}\right)^{1/2}\left(\rho_0/\rho\right)^{1/2}\frac{1}{(C_T/\sigma)^{1/2}} \tag{7}$$

Sissingh[7] has shown that the static efficiency of a rotor is a maximum when $C_T/\sigma = 0.20$. This relation is very nearly true for any reasonable rotor design and is roughly true even at moderate forward speeds. Marked improvement in airfoil characteristics may result in some change in the optimum thrust coefficient, but the relation is sufficiently accurate to determine the optimum rotor speed at low rates of advance at any given flight condition. The rotor speed will be determined by this relation at some flight condition, probably hovering at sea level, and the rotor r.p.m. at other flight conditions will probably follow from considerations of engine operation. Substituting the value of C_T/σ, the optimum speed is

$$\omega = \frac{36.6}{R^2}\left(\frac{W}{\sigma}\right)^{1/2}\left(\frac{\rho_0}{\rho}\right)^{1/2} \tag{8}$$

Profile Torque

The profile torque of a rotor is

$$Q_R = \frac{1}{2\pi}\int_0^{2\pi}\int_0^R \delta(\rho/2)bcr\,dr\,(\omega r + U\sin\psi)^2 d\psi$$

where U is the velocity in the plane of the rotor. $U = V\cos\alpha'$. Integrating

$$Q_R = (\rho/2)(\delta/4)\,\sigma\pi\omega^2R^5\,(1+\mu^2)$$

The power absorbed by the profile drag is

$$P_R = \omega Q_R = (\rho/2)(\delta/4)\,\sigma\pi\omega^3R^5\,(1+\mu^2) \tag{9}$$

Sissingh[6, 7] has shown that the mean lift coefficient is approximately

$$C_L = (3/B^3)(C_T/\sigma)$$

from which

$$C_L = 3.5\,(C_T/\sigma) \tag{10}$$

δ in Eq. (9) is the profile drag coefficient of a rotor blade section at the section lift coefficient obtained from Eq. (10). This relation for the mean lift coefficient is, to be sure, only an approximation and is derived for the case of static lift, but it provides a means of estimating the effective blade profile drag coefficient. For this purpose it is sufficiently accurate and tends to be conservative for flight at moderate speeds.

Power Available for Thrust

The power left for producing thrust after the losses are accounted for is

$$P_i = 550K \text{ b.hp.} - P_R \tag{11}$$

The power P_i is the power available to the rotor to produce a jet of air. The power imparted to the jet is equal to the thrust times the total velocity in the direction of the thrust.

$$P_i = T(u + V \sin \alpha')$$

and since $T = W$

$$P_i = Wu + WV \sin \alpha' \tag{12}$$

Equating Eqs. (11) and (12) and dividing by Wu_0,

$$\frac{u}{u_0} + \frac{V}{u_0} \sin \alpha' = \frac{550K \text{ b.hp.}}{Wu_0} - \frac{P_R}{Wu_0} \tag{13}$$

The left-hand member of this equation is, from Eq. (3), equal to S. Then

$$S = \frac{550K \text{ b.hp.}}{Wu_0} - \frac{P_R}{Wu_0} \tag{14}$$

Substituting the value of P_R from Eq. (9), putting the value of ω from Eq. (6) in the expression for P_R, and substituting the value of u_0 from Eq. (2),

$$S = \frac{550K \text{ b.hp.}}{Wu_0} - \frac{B}{2(C_T/\sigma)^{3/2}} \frac{\delta}{\sqrt{\sigma}} (1 + \mu^2) \tag{15}$$

Eq. (15) is the useful equation for performance estimation. From these equations it is evident that the useful parameter S has two meanings. It is the ratio of the total axial velocity component to the axial velocity when $V = 0$, and it is also a measure of the power available for the production of thrust after all losses are accounted for. It appears in the latter sense in Eq. (15), which can be easily evaluated. The quantity μ may not be known at the beginning of a specific performance calculation, but its effect is small and an assumed value is quite satisfactory. Having calculated a value of S, Eq. (4) or Fig. 2 representing Eq. (4) gives a series of corresponding values of V/u_0 and u/u_0. These values define a series of flight conditions. Then the angle α' is defined by the equation

$$S = (V/u_0) \sin \alpha' + (u/u_0) \tag{16}$$

Flight Path

The flight path is, from Fig. 1,

$$\alpha = \alpha' - \gamma = \alpha' - \frac{D}{T} = \alpha' - \frac{D}{W} \tag{17}$$

where D is the total drag of the machine. $D = D_R + D_P$.

The horizontal component of the parasite drag of the machine is

$$D_P = f(\rho/2)U^2 = f(\rho/2)(V \cos \alpha')^2$$

The drag due to the profile drag of the rotor blades is

$$D_R = \frac{1}{2\pi} \int_0^{2\pi} \int_0^R \delta(\rho/2)bc\,dr\,(U \sin \psi + \omega r)^2 \sin \psi \, d\psi$$

$$= (\rho/2)(\delta/2)bcU\omega R^2$$

$$= (\rho/2)(\delta/2)\sigma\pi U\omega R^3$$

Adding D_R and D_P and dividing by W

$$D/W = \frac{\rho U}{2W}\left(\frac{\delta}{2}\sigma\pi\omega R^3 + fU\right)$$

$$= \frac{\rho V \cos \alpha'}{2W}\left(\frac{\delta}{2}\sigma\pi\omega R^3 + fV \cos \alpha'\right) \tag{18}$$

The flight path angle is then, from Eqs. (17) and (18),

$$\alpha = \alpha' - \frac{\rho V \cos \alpha'}{2W}\left(\frac{\delta}{2}\sigma\pi\omega R^3 + fV \cos \alpha'\right) \tag{19}$$

The angles are in radians. The equation appearing in the summary gives the angle in degrees.

Vertical Climb

In vertical climb, Eq. (3) reduces to

$$\frac{V}{u_0} + \frac{u}{u_0} = S \quad \text{or} \quad \frac{u}{u_0} = S - \frac{V}{u_0} \tag{20}$$

Writing Eq. (4) in the form

$$\left(\frac{V}{u_0}\right)^2 = \left(\frac{u_0}{u}\right)^2 + \left(\frac{u}{u_0}\right)^2 - 2\left(\frac{u}{u_0}\right)S$$

the value of u/u_0 can be substituted from Eq. (20). Solving for V/u_0 in terms of S, the solution is $V/u_0 = S - (1/S)$ or $V = u_0[S - (1/S)]$.

Since V is a vertical velocity, the vertical rate of climb in feet per minute is

$$V_{c_0} = 60u_0[S - (1/S)] \tag{21}$$

the value of S being taken for the condition $\mu = 0$.

From this equation, it is apparent that the hovering condition is $S = 1.00$.

Evaluation of K

The power losses in per cent of total b.hp. are approximately as follows:

Transmission losses	$3\frac{1}{2}$ per cent
Cooling (blower) power	$4\frac{1}{2}$ (unsupercharged)
Slipstream rotation	5
Tail rotor	6
Total loss	19 per cent

For supercharged engines, cooling power may be about 3 per cent at sea level.

$$K = 1.00 - 0.19 = 0.81$$

The most convenient procedure is to estimate the value of K for one flight condition and use the same value for all conditions. A method of estimating the tail rotor power loss follows.

Estimation of Tail Rotor Power

(For helicopters with torque counteracting auxiliary rotors.) The main rotor torque is

$$Q = P/\omega = 550K \text{ b.hp.}/\omega \tag{22}$$

The thrust required at the control rotor to balance the main rotor torque is

$$T_T = Q/l \tag{23}$$

where l is the moment arm of the tail rotor about the main rotor axis. The power required by an airscrew to deliver a given static thrust is

$$550\eta_S \text{ b.hp.} = T\sqrt{\frac{T}{2\rho\pi R^2}} \tag{24}$$

where η_S is the static thrust efficiency, which may be taken as equal to 0.70. Substituting Eqs. (22) and (23) in Eq. (24),

$$\text{b.hp.}_T = \left(\frac{550K \text{ b.hp.}}{\omega l}\right)^{3/2} \frac{1}{550 \times 0.7\sqrt{2\rho\pi R_T^2}}$$

Simplifying,

$$\text{b.hp.}_T = \frac{548}{D_T}\left(\frac{K \text{ b.hp.}}{\omega l}\right)^{3/2}\left(\frac{\rho_0}{\rho}\right)^{1/2} \tag{25}$$

where D_T is the diameter of the control rotor and ω is the speed of the main rotor. The diameter and rotational speed of the tail rotor should be adjusted so that C_T/σ is approximately equal to 0.20 for the hovering condition. K in Eq. (25) is, of course, dependent on b.hp.$_T$, but an estimated K satisfies Eq. (25) with sufficient accuracy to obtain b.hp.$_T$ and the resulting new and more accurate value of K. The loss of power due to the tail rotor in per cent is b.hp.$_T$/b.hp. Then

$$K = 1.00 - \Sigma \text{ losses}$$

Procedure

The equations as presented do not give maximum speeds and rate of climb directly but give the speed along the flight path and the angle of the flight path for a series of flight stages. The determination of maximum rate of climb, maximum horizontal speed, etc., necessitates plotting a speed polar (V_c vs. V_h) from which all phases of performance at a given altitude and power can be read directly.

The procedure in calculating a point on the performance curve is as follows:

1. Solve Eq. (5) for u_0.
2. Knowing the rotor speed ω or using the approximately optimum value of Eq. (8), calculate the blade loading coefficient C_T/σ.
3. From the polar of the rotor airfoil section, obtain the blade profile drag coefficient $\delta = C_{D_0}$ at the average blade lift coefficient (Eq. (10)).
4. Compute S from Eq. (15).

The value of μ is as yet unknown, but its effect is small and with a little practice its value can be accurately estimated for each point on the performance curve. When the rotor speed is that prescribed by Eq. (8), Eq. (15) reduces to

$$S = \frac{550K \text{ b.hp.}}{Wu_0} - 5.31\frac{\delta}{\sqrt{\sigma}}(1 + \mu^2)$$

5. Referring to Fig. 2, choose corresponding values of u/u_0 and V/u_0 at the computed value of S. Determine V.
6. Check the assumed value of μ.

$$\mu = V\cos\alpha'/\omega R$$

7. Then use the value of $\sin\alpha'$ from Eq. (16).
8. The flight path angle is (see Eq. (19))

$$\alpha = \alpha' - 0.0681\frac{V\cos\alpha'}{(\rho_0/\rho)W}\left(\frac{\delta}{2}\sigma\pi\omega R^3 + fV\cos\alpha'\right)$$

9. Rate of climb in feet per minute is

$$V_c = 60V\sin\alpha$$

10. The corresponding horizontal component of speed in m.p.h. is

$$V_h = 0.682V\cos\alpha$$

Example

To illustrate the results of the performance equations, the performance of a representative helicopter has been calculated and plotted in Fig. 3. The climb curve for the corresponding airplane with both a fixed and a variable pitch propeller has also been calculated. The corresponding airplane has been taken as one having the same brake horsepower, same span, same weight, and comparable care in minimizing parasite drag. (The parasite drag of the helicopter is taken equal to 1.25 times the difference between the total parasite drag of the airplane and the airplane wing profile drag. $C_{D_p} = 0.010$.)

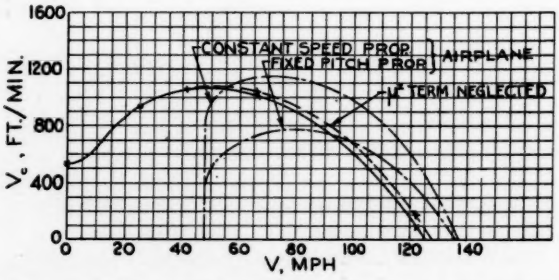

FIG. 3. Typical helicopter performance curve and performance of the corresponding airplane, both at sea level.

Curves have been calculated both with and without the μ^2 term included in the value of S in order to illustrate the magnitude of its effect. It is evident that for approximate work it may be neglected.

Characteristics of the machines used as examples:

Airplane		Helicopter	
W	= 1,500 lbs.	W	= 1,500 lbs.
b	= 33.6 ft.	D	= 33.6 ft.
b.hp.	= 100	b.hp.	= 100
W/S	= 10.0 lbs. per sq.ft.		
C_D	= 0.030		
f	= 4.50 sq.ft.		
(Residual drag f_R = 3.00 sq.ft.)		f	= 1.25 × 3.00 = 3.75 sq.ft.
$\eta_{max.}$	= 0.83	σ	= 0.070 K = 0.81
		δ	= 0.0125 C_T/σ = 0.20

REFERENCES

[1] Glauert, H., *Horizontal Flight of a Helicopter*, R. & M. No. 1157.

[2] Hohenemser, K., *Performance of Rotating Wing Aircraft*, N.A.C.A. T.M. No. 871, 1938.

[3] Knight, M., *General Flight Analysis of the Helicopter*, presented at the Rotating Wing Aircraft Session, Tenth Annual Meeting, I.Ae.S., New York, January 29, 1942.

[4] Knight, M., and Hefner, R. A., *Static Thrust Analysis of the Lifting Airscrew*, N.A.C.A. T.N. No. 626, 1937.

[5] Küssner, H. G., *Helicopter Problems*, N.A.C.A. T.M. No. 827, 1937.

[6] Sissingh, G., *Contribution to the Aerodynamics of Rotating Wing Aircraft*, N.A.C.A. T.M. No. 921, 1939.

[7] Sissingh, G., *Contribution to the Aerodynamics of Rotating Wing Aircraft, Part II*, N.A.C.A. T.M. No. 990, 1941.

[8] Squire, H. B., *The Flight of a Helicopter*, R. & M. No. 1730, 1936.

[9] Wheatley, J. B., *An Aerodynamic Analysis of the Autogiro Rotor with Comparison Between Calculated and Experimental Results*, N.A.C.A. T R. No. 487, 1934.

Letter to the Editor

Dear Sir:

In a letter to the editor from Mr. Manley on "Pendulum-Type Vibration Absorbers" (*Journal of the Aeronautical Sciences*, January, 1943), he pointed out the incorrectness of the assumption of the "reduced system" made in the writer's paper in the JOURNAL, July, 1942. He corrected this by adding one more equation of motion for the propeller and showed the deviation of my result from his correct one.

However, two further points have to be considered: One is the damping effect of air on propeller, and the other is the assumption, $mk^2 << I_2$. The latter assumption has been used in the writer's paper and also employed by Mr. Manley in his work. This assumption is evidently not true, because my first approximation already indicates a value of μ lying between 0.4 and 0.5 and his considerations also indicate that μ should be made as large as possible. From this point of view, Mr. Manley's calculation is also unsatisfactory.

Regarding the damping effect of air on propeller, it could be taken into account by adding a term $-c\dot{\theta}_1$ on the right side of the third equation of (1) in Mr. Manley's letter, where c is the damping constant depending upon the propeller speed (see Den Hartog's *Mechanical Vibrations*, 2nd Edition, p. 251; McGraw-Hill Book Co., Inc., New York, 1940). Then the amplitude of I_2 can be expressed as

$$\frac{M_0}{\theta_m} = \sqrt{\left[K - (I_2 + mk^2)p^2 - \frac{mL(R+L)^2p^4}{R\Omega^2 - Lp^2} - \frac{K^2(K - I_1p^2)}{(K - I_1p^2)^2 + c^2p^2}\right]^2 + \left[\frac{Kcp}{(K - I_1p^2)^2 + c^2p^2}\right]^2}$$

By putting it into nondimensional form, the following equation is obtained:

$$\frac{\theta_{st.}}{\theta_m} = \sqrt{\left[1 - r_1(1+r_2)g^2 - r_1(1-r_2)g^2\frac{n^2}{N^2 - n^2} - \frac{1-g^2}{(1-g^2)^2 + f^2}\right]^2 + \left[\frac{f}{(1-g^2)^2 + f^2}\right]^2}$$

where

$$N^2 = \frac{R}{L} \qquad r_2 = \frac{mk^2}{I_2} \qquad r_1 = \frac{I_2}{I_1}$$

$$f = \frac{p}{\Omega_e} \qquad g = \frac{p}{\Omega_1} \qquad n = \frac{p}{\Omega}$$

$$\Omega_e = \frac{K}{c} \qquad \Omega^2_1 = \frac{K}{I_1} \qquad \theta_{st.} = \frac{M_0}{K}$$

The above equations may give a better understanding of the engine-propeller vibration characteristics.

In addition, there is one further remark to be made. The above equations are valid only for the case of direct-drive propellers. Modern high-performance airplanes are practically all equipped with geared propellers. Theoretic investigation of this case involves no new principles, except more equations have to be handled. The calculations will be quite lengthy and cumbersome.

A. H. SHIEH
Pasadena, Calif.

SUGGESTIONS FOR CONTRIBUTORS TO THE PUBLICATIONS *of the* INSTITUTE *of the* AERONAUTICAL SCIENCES

The Institute of the Aeronautical Sciences invites both members and nonmembers from any country to submit papers for publication in the JOURNAL OF THE AERONAUTICAL SCIENCES and the AERONAUTICAL ENGINEERING REVIEW. The Institute, following the practice of other societies, does not pay for contributions.

The following directions for the preparation of papers, if followed by authors, will save correspondence, avoid the return of papers for changes, minimize the work of preparation for the printer, and save the expense due to the charges made for "author's corrections."

MANUSCRIPTS: Papers must be written in English, in original typewriting on one side only of white paper sheets, consecutively numbered, and be double or triple spaced with wide margins. Manuscripts should be prepared with great care so that they will be typographically accurate. Paragraphing should be given special attention. Papers should be written in the third person, reference to the writer being made as "the author." Avoid the use of the words "I," "we," and "you." Blueprint copies of papers are unacceptable as it is impossible to mark directions to the printer on them. Correcting, changing, or adding to papers after they are in type is costly. It is, therefore, imperative that papers submitted be in final form. Typographical errors may be corrected on proofs, but if authors wish to add material, they may do so at their own expense. In mailing, drawings may be rolled, but manuscripts should be sent flat. Send by first class mail (register if you wish for your own protection) to the Editorial Office, Institute of the Aeronautical Sciences, 1505 RCA Bldg West, Rockefeller Center, New York City. All manuscripts will be examined by the Editorial Committee and by the Editor. Authors will be advised as promptly as possible (usually two to three weeks) whether the paper is acceptable for publication.

TITLES: The title of the paper should be brief. The name and initials of the author should be written as he prefers. The use of the full name of an author is advocated because of the frequent duplication of initials and surnames which sometimes makes it difficult to establish the identity of the author. This is particularly important for large annual indexing and abstracting services. All titles and degrees or honors are omitted. The name of the organization with which the author is associated should be placed after his name on the same line. The date on which the paper is received will be inserted by the Editor.

SUMMARIES OR ABSTRACTS: An abstract to be printed at the beginning should accompany each article. It should be adequate as an *index* and as a *summary*. It should contain a statement of major conclusions reached, since summaries in many cases constitute the only source of information used in compiling scientific reference indexes. Abstracts printed in other journals, especially foreign, in most cases, consist of summaries from printed papers. The summary should explain as adequately as possible the major conclusions to a nonspecialist in the subject. The summary should contain from 100 to 300 words, depending on the length of the paper.

SUB-HEADINGS: Sub-headings should be inserted by the author at frequent intervals. The work of editorial preparation will be simplified by the author providing many sub-headings. Owing to the breaking of columns and the insertion of illustrations, some of the sub-headings may have to be omitted.

SHORTENING OF PAPERS: Some papers, at the end, fill in only a portion of a page. This leaves much wasted blank space as succeeding articles are started at the top of a page. Authors should indicate by notation on the left-hand side of the page what matter may be omitted when "runovers" occur. This request is important as the Journal cannot afford in the future, as it has in its earlier issues, to have blank half pages or more at the end of papers.

MATTER USUALLY DELETED: Acknowledgments of assistance in preparation of paper, except by collaborators. Photographs or illustrations of little technical interest and not showing advances in general practice. Too detailed tabular matter (general results of such tables may be included in the text). Lengthy descriptions of materials or processes or of preliminary experiments or theories which preceded final results; salient features only are of interest.

REFERENCES AND FOOTNOTES: References should appear as footnotes only, numbered consecutively, grouped together at the end of the manuscript. The arrangement should be as follows: (for books)—[1] Durand, W. F., *Aerodynamic Theory*, 1st Edition, Vol. 1, p. 23; Julius Springer, Berlin, 1934. (For magazines)—[1] Englund, C. R., Crawford, A. B., and Mumford, W. W., *Some Results of a Study of Ultra-Short-Wave Transmission Phenomenon*, Proc. I. R. E., Vol. 20, No. 12, pp. 481 and 482, March, 1933. Please give Author, Title, Edition, Volume, page, publisher and date of publication as indicated. Omission of one required fact causes much extra editorial work and possible inaccuracies. All references are grouped at the end of the article.

ILLUSTRATIONS: Illustrations should accompany manuscripts and each should always be referred to in the text, preferably by number. Drawings or graphs should not be larger than 12×16 inches, and must be made with jet black India Ink on white paper or tracing cloth, the latter being preferred. *Do not use typewriter for lettering.* The smallest lettering on 8×10 inch figures should be no less than $1/4$ inch high. Cross-section paper (white with black lines) may be used, but should not have more than 4 lines per inch. If finer ruled paper is used, the major division lines should be drawn in with black ink, omitting the finer divisions. In the case of finely ruled paper, only blue-lined paper can be accepted. *Tracing paper and blueprints* are not acceptable. Lettering and all markings must be large enough to be readable after reduction. Mail rolled or flat, never fold. Drawings which cannot be reproduced (including pencil drawings) will be returned to the author for redrawing, thus delaying publication of the paper. Photographs should be very distinct and show clear black and white contrasts. They must be on glossy white paper. Avoid round and oval photographs.

CAPTIONS AND LEGENDS: Legends or captions must accompany each drawing or photograph submitted. If written on the drawing or photograph, they should be placed below and well outside the part to be reproduced. It is better to place them on separate sheets of paper pasted to the back of the drawings or photographs. Each table should have a caption such as Table 1, Table 2, Table 3, etc. Captions should be complete in themselves so as to make the data intelligible to the reader without reference to the text. A duplicate list of captions for figures should be included as the last page of the manuscript. Use "Fig. 1" (not Figure 1), Figs. 3 and 4, etc., in both the text and the numbering of illustrations. In the text, "Eq. (1)," or "Eqs. (1) and (2)" are preferable to "Equation (1)." In captions and legends, except for "Fig." and "Eq." and table headings, write all words in full; do not abbreviate. Avoid placing explanatory written matter in the drawings; it should be in the text.

MATHEMATICAL WORK: Only the very simplest formulas should be typewritten; all others should be very carefully written in pen and ink, the writing to be large enough so that ample room is provided to mark mathematical matter for the printer. A considerable space for marking should be allowed above and below all equations. All complicated equations should be repeated on separate sheets with plenty of space left for marking. The solidus should be used for simple fractions appearing within the text. Make all expressions clear to the typesetter. Greek letters used in formulas should be clearly designated by name on the margin of the manuscript. All symbols should be clearly written and carefully checked. The difference between capital and lower-case letters should be clearly distinguished and care taken to avoid confusion between zero (0) and the letter (o), between the numeral (one) and the letter (ell) and the prime ('), between alpha and a, kappa and k, u and mu, v and nu, n and eta. All subscripts and exponents should be clearly marked and dots and bars over letters or mathematical expressions should be avoided. Avoid complicated exponents and subscripts. When it is necessary to repeat a complicated expression, it should be represented by some convenient symbol.

NOMENCLATURE AND ABBREVIATIONS: The National Advisory Committee for Aeronautics Nomenclature should be used in preference to any others. Standard abbreviations should be used, and it should be noted that most abbreviations are lower case, such as m.p.h., b.m.e.p., i.hp., b.hp., hp., . . . etc.